The mechanisms and applications of a nucleotide-based heart failure therapy

Jason David Murray

A dissertation

submitted in partial fulfillment of the

requirements for the degree of

Doctor of Philosophy

University of Washington

2019

Reading Committee:

Michael Regnier, Chair

David Marcinek

Farid Moussavi-Harami

Program Authorized to Offer Degree:

Physiology and Biophysics

University of Washington

Abstract

The mechanisms and applications of a nucleotide-based heart failure therapy

Jason David Murray

Chair of the Supervisory Committee:
Professor Michael Regnier
Department of Bioengineering

The naturally-occurring nucleotide 2-deoxy-ATP (dATP) is known to increase the amount of force produced by cardiac muscle when used as a substrate in place of ATP. Cytosolic concentration of dATP can be elevated by expressing both subunits of the enzyme ribonucleotide reductase (RNR), and overexpression of RNR in the heart has been previously shown to increase the magnitude of pressure development in the heart as well as increase the rates of contraction and relaxation in transgenic mice as well as virally-transduce rodent and large-animal models. The first aim of this dissertation utilizes Brownian dynamics simulations in concert with small-angle x-ray diffraction analysis of sarcomere structure to demonstrate that dATP induces structural changes in the conformation of myosin that increases its electrostatic affinity for actin and leads to an altered structural confirmation at rest that resembles changes caused by calcium-mediated activation. The second aim applies our therapeutic to a disease model and explores possible changes in skeletal muscle activation through a combinatorial gene therapy for a mouse

model of Duchenne muscular dystrophy. Overexpression of RNR in concert with an artificial microdystrophin construct improved fractional shortening in cardiomyocytes but did not alter the overall force or kinetics of hindlimb muscle in either our disease model or in a mouse model of transgenic overexpression of ribonucleotide reductase. The third aim explores methods by which dATP can be elevated. We describe cardiac function after overexpression of Rrm1 and Rrm2B (RNRB), an isoform of the small subunit of RNR that has not been characterized in the heart. RNRB elevates cardiomyocyte dATP in a transgenic mouse model to the same degree as RNR, resulting in increases in cardiac function on multiple biophysical scales. Calcium handling was also altered in cardiomyocytes through an increase in the rate of calcium signal decay during contraction, a novel result which has not been previously described. These changes were reproducible *in vitro* in adult rat cardiomyocytes overexpressing RNRB through virally-mediated transduction in culture. Identifying a form of RNR that can be stably overexpressed in cardiomyocytes is an important step towards developing a therapeutic based on elevation of dATP.

TABLE OF CONTENTS

LIST OF FIGURES

LIST OF TABLES

ACKNOWLEDGEMENTS

There are a large number of people without whom this work wouldn't have been possible. I'd like to first thank my advisor Dr. Michael Regnier for supporting me these past six years, helping me to become a better scientist, and guiding me to the finish line. Dr. Farid Moussavi-Harami has been working with me every step of the way and there aren't sufficient words to express my gratitude for his help. I'd also like to thank the rest of my supervisory committee, Drs. David Marcinek, Qinghang Liu, Charles Asbury, and April Stempien-Otero for their time and mentorship.

I've worked with a lot of great scientists. Many great HAMMies have helped me to become a better experimentalist and communicator. Galina Flint, An-Yue Tu, and Masha Razumova in particular have helped tremendously. Joe Powers and Chen-ching Yuan did a fantastic job taking the lead on our x-ray diffraction work. Sabrina Do has been a fantastic assistant. It's been a great pleasure working with Guy Odom on projects relating to gene therapy and muscular dystrophy. I'd also like to acknowledge the contributions of Tom Irving, Weikang Ma, and Jil Tardiff and thank them for their insight and for welcoming me into their respective laboratories. And I'd like to thank Paul Janssen for introducing me to muscle biology.

Lastly, I have a fantastic set of friends and family that have supported me. Tony and Joyce Murray have always loved me and believed in me. Yoni Browning, Devon Simpson, Will Dawkins, and Karl Mitchell have made Washington feel like home and supported my cycling habit. I blame Nick Waldo and Erin McLean for getting me into sailing. And I need to thank Alainna Brown for keeping me focused on what's most important and inspiring me to always be better.

DEDICATION

For my parents

Chapter 1. INTRODUCTION

1.1 HYPOTHESES AND GOALS

The overarching goal of this work is to advance the development of 2-deoxy-ATP as a therapeutic for heart failure via targeted overexpression of ribonucleotide reductase. Aim 1 concerns the mechanisms of elevated function in cardiac muscle by dATP and tests the hypothesis that enhanced force production is due to increased weak binding of myosin to actin caused by increased electrostatic interaction when dATP is bound to myosin. Aim 2 focuses on translating these findings from biophysical discoveries to therapeutic use, and potential therapeutic use in skeletal muscle using virally-mediated overexpression of RNR along with engineered dystrophin in a mouse model of Duchenne muscular dystrophy. Aim 3 investigates the effects of transgenic overexpression of the Rrm1 and Rrm2B subunits of ribonucleotide reductase and its comparison to Rrm2 for sustained transduced overexpression in cardiomyocytes.

1.1.1 Aim 1: The structural basis of functional augmentation by dATP

This aim is separated into two chapters centered on activation and relaxation, respectively. We have repeatedly demonstrated that 2-deoxy-ATP (dATP) can be used as a substrate for force generation by myosin, and that replacement of ATP with dATP increases force production in rodent, porcine, and human cardiac muscle(1–5). Previous molecular dynamics simulations suggest that when dATP (more precisely, dADP*P_i after hydrolysis of the dATP molecule by myosin ATPase) is bound to myosin before the power-stroke, the conformation of the myosin head changes such that an increased number of positive charges are exposed on the actin-binding surface(6). We hypothesized that this increases the affinity of myosin for actin via increased electrostatic interactions between the thick and thin filaments even at rest, increasing force via increased cooperativity and recruitment of myosin heads. To test this hypothesis, we performed Brownian dynamics simulations to model interaction between myosin and actin when bound to ADP*P_i and dADP*P_i. Concurrently, we utilized the Advanced Photon Source at Argonne National Laboratory to perform x-ray diffraction experiments of demembranated cardiac muscle incubated in ATP or dATP. Solutions of differing ionic strengths were used to test whether altering electrostatic interactions is sufficient to alter the weak (non-Ca^{2+}-dependent) binding of myosin to

actin. This is a highly collaborative project that would not have been possible to complete without a large and capable team. All Brownian dynamics simulations were done by Kim McCabe. I made significant contributions to the design, troubleshooting, execution, and discussion of the x-ray diffraction experiments using skinned cardiac muscle along with Joe Powers and Chen-Ching Yuan, who completed the analysis of the diffraction patterns. Saffie Mohran and Romi Castillo performed the *in vitro* motility experiments comparing myosin-ATPase activity of ATP and dATP over a range of ionic strength.

1.1.2 Aim 2: Elevated dATP in skeletal muscle

dATP has been shown to increase calcium sensitivity in skeletal muscle without increasing force production at maximum calcium. This pilot study tests the efficacy of delivering RNR to both cardiac and skeletal muscle in combination with an engineered "microdystrophin" to preserve muscle function in a mouse model of Duchenne muscular dystrophy. While the effect of dATP on cardiac muscle has been well characterized, these are the first *in vivo* measurements of virally-transduced skeletal muscle with elevated dATP. This project is a collaboration with Drs. Jeff Chamberlain, Steve Hauschka, Guy Odom, and Dave Marcinek.

1.1.3 Aim 3: Overexpression of multiple RNR isoforms enhances cardiac function

Cytosolic concentration of dATP can be elevated by overexpressing the enzyme ribonucleotide reductase (RNR), which is the rate-limiting step for *de novo* synthesis of dNTPs. RNR comprises the subunits Rrm1 and Rrm2, of which Rrm2 is rate-limiting in formation of an active complex. Previous studies have shown that overexpression of both subunits significantly elevates cytosolic concentration of dATP to approximately 1% of the available ATP pool, which is sufficient to increase the rate and magnitude of left ventricular pressure development in both transgenic and virally-transduced animal models. Our experiments use adeno-associated virus (AAV) with cardiomyocyte-specific promotors to transduce the heart *in vivo*. In many of these studies Rrm1 overexpression has been stable, but Rrm2 levels have varied significantly between treated individuals. We hypothesized that this was due to degradation of the protein by the ubiquitin-proteasome pathway, which regulates RNR activity by mediating Rrm2 levels in a cell cycle-dependent manner. This aim investigates the feasibility of using different isoforms of RNR to engineer a more stable method of overexpressing the enzyme and thereby elevating dATP to a

level that will increase cardiac function with the eventual goal of developing dATP as a therapeutic for cardiomyopathy. We measured [dATP] and cardiac performance of mice overexpressing Rrm1 and Rrm2B *in vivo, ex vivo,* and with isolated cardiomyocytes *in vitro.* We then used adenovirus to transduce isolated adult rat cardiomyocytes *in vitro* with Rrm1 along with either Rrm2, Rrm2B, or Rrm2 with an engineered mutation that impairs its ability to be ubiquitinated for degradation by the proteasome to directly compare the efficacy of different isoforms of the small subunit for therapeutic use in cardiomyocytes and the importance of Rrm2 degradation via the ubiquitin-proteaseome pathway.

1.2 BACKGROUND

1.2.1 Heart failure and cardiomyopathy

Heart failure is the inability for the heart to keep up with the body's demand and affects an estimated 6 million Americans. Despite advances in care, 5-year mortality after a heart failure diagnosis remains over 50% (7). The most prominent risk factors are hypertension, obesity, and advanced age, and incidence is expected to increase in the coming decades due to the aging population. Roughly half of these cases are heart failure with preserved ejection fraction (HFpEF), although both HFpEF and HF with reduced ejection fraction (HFrEF) have seen steady increases in cases over the years(7). Aging is a particularly challenging topic because it affects everyone and is a significant risk factor for cardiac dysfunction, yet the process is still poorly understood and does not affect everyone equally. Systolic function is largely preserved in the healthy elderly, but diastolic dysfunction becomes more common as the heart remodels itself during the aging process. Heart weight and myocardial thickness increase with age, primarily due to a decrease in the total number of cardiomyocytes and hypertrophy of those that remain, which leaves aged hearts more vulnerable to stress and less able to recover from injuries such as myocardial infarction (8, 9). Studies in both animal models and human trials have found increased cardiac fibrosis (10) and increased myocyte stiffness (11) with advanced age. Calcium handling is also impaired in aging cardiomyocytes; SERCA activity and expression levels are both reduced with aging, leading to reduced amplitude of calcium transients, higher sarcoplasmic [Ca^{2+}], and further impaired relaxation (12, 13). Because HFpEF accounts for approximately 50% of patients hospitalized for heart failure (14), it is important that potential therapies for age-related heart failure address issues

in diastole along with systole. dATP is unique in that it is the only known compound which increases the kinetics of both contraction and relaxation in cardiac muscle; other known inotropes such as omecamtiv mecarbil generate increased force at the expense of prolonged relaxation.

1.2.2 The myosin cross-bridge cycle

Muscle contraction is driven by cyclic interactions between myosin and actin within the thick and thin filaments of the sarcomere. in which chemical energy from the hydrolysis of ATP is transduced to mechanical energy and myocyte shortening (15). When the regulatory elements of the thin filament are activated by calcium and ATP is available for hydrolysis, myosin heads will continually bind with actin, perform mechanical work, and release (Figure 1.1). There is strong evidence that strong actin-myosin interaction in cardiac muscle can further displace tropomyosin along the thin filament and allow for cooperativity along the filament wherein the formation of one actin-myosin "crossbridge" increases the likelihood of formation of additional cross bridges and enhancing the force of the twitch (16). This makes myosin an attractive target for potential therapeutics in heart failure. Many small molecules that act directly on the sarcomere are under currently investigation. The most prominent example, omecamtiv mecarbil, enhances cooperativity in cardiac myosin by prolonging the actin-myosin binding phase and is in phase 3 clinical trials at the time of this writing (17–25).

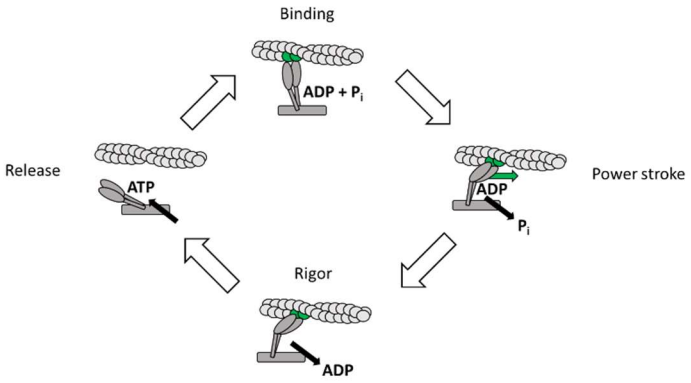

Figure 1.1: The myosin crossbridge cycle

1.2.3 X-ray diffraction of striated muscle

X-ray diffraction is a powerful tool for visualizing the structure of the sarcomere. The myofilaments of striated muscle are arranged in an extremely convenient quasi-crystalline lattice that allows (with a beam of sufficient strength) visualization of nanometer-scale structural details to be imaged by x-ray diffraction. Details such as interfilament lattice spacing, radial distribution of mass, and intra-filament myosin head spacing can be divined through analysis of diffraction patterns along two distinct planes: equatorial and meridional.

The meridional axis features a series of layer lines arising from axial periodicity along the filaments, especially the myosin layer lines (26). Reflections on the equatorial axis reflects the relationship between filaments. Of particular interest in vertebrate muscle are two points termed (1,0) and (1,1) reflections. The distance between (1,0) reflections is directly related to the spacing between filaments in the muscle's crystalline lattice (27). The relative intensity of (1,0)/(1,1) is related to the radial distribution of mass between the thick and thin filaments; i.e. the ratio indicates the position of the S1 myosin heads relative to the filament backbone. This is supported by the increase in (1,1) and decrease in (1,0) intensity during activation (28).

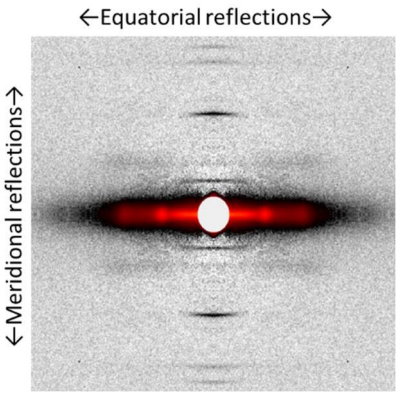

Figure 1.2: An example x-ray diffraction pattern from cardiac muscle

1.2.4 2-deoxy-ATP enhances contractility in cardiac muscle

Another potential small molecule therapeutic is the naturally occurring nucleotide 2-deoxy-ATP (dATP), which has been extensively studied in the Regnier lab for the past 20 years. Cardiac myosin is able to bind with dATP in place of ATP, which results in an increase in both the rate and magnitude of tension development in a variety of experimental systems in rodent, porcine, canine, and human tissues (1, 5, 29–32) by altering the dynamics of myosin-actin crossbridge formation and increasing myosin recruitment (6). Indeed, only a small increase in dATP content is needed for significant improvement in both systolic and diastolic parameters; making it a candidate for improving both systolic and diastolic heart failure.

dATP is a naturally occurring molecule in every living cell. It is an essential component of DNA, and its concentration oscillates through the cell cycle, being highest in S-phase proceeding and during DNA synthesis. In non-dividing cells like cardiomyocytes dATP levels are quite low, about 5 μM. This can be elevated by overexpressing the enzyme ribonucleotide reductase (RNR). Our group has shown repeatedly that overexpression of RNR in cardiomyocytes either transgenically or by viral vector elevates cytosolic concentrations of dATP to approximately 1% of the available ATP pool, which is sufficient to alter cardiac contractility (2–4, 33).

1.2.5 Structure and regulation of ribonucleotide reductase

Structurally, the active form of RNR is a heterotetramer with two functional subunits, themselves being homodimers. The large subunit (Rrm1) contains the catalytic site in which a nucleotide diphosphate (NDP) is reduced to a deoxy-nucleotide diphosphate (dNDP) and a regulatory site by which the enzyme's activity is altered by the relative ratios of ATP and dATP (34).

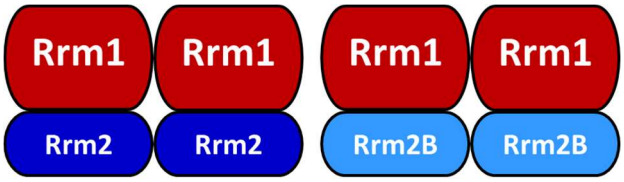

Figure 1.3: Rrm1 can form a functional complex with two different isoforms of the small subunits.

There are two different isoforms of the small subunit encoded by separate genes and regulated by different pathways, designated Rrm2 and Rrm2B. Rrm2 levels fluctuate with the cell cycle in actively dividing cells, reaching a peak in S-phase, after which it is degraded by the ubiquitin-proteasome system.

Virally-induced overexpression of Rrm1 in our hands is stable, but we have seen high variability in the Rrm2 and dATP levels in multiple disease models. We hypothesized that variability was due to protein degradation via the ubiquitin-proteaseome system and found that pharmacological inhibition of proteasome activity leads to increased expression of Rrm2 and [dATP] in virally-transduced cardiomyocytes in vitro (Regnier lab unpublished data). We are now exploring the effectiveness of different small subunits to develop an improved method for elevating dATP as a therapeutic.

Rrm2B is an alternate isoform of the small subunit that also forms a complex with Rrm1. Levels of Rrm2B are more consistent in post-mitotic cells than Rrm2, and it lacks the amino acid sequence that is targeted by the ubiquitin-conjugating enzyme. Rrm2B is necessary for supplying dNTPs for the synthesis of mitochondrial DNA, and thus even quiescent cells continue to express it.

1.2.6 Cardiac gene therapies

Our goal is to develop an improved vector to enable stable and consistent overexpression of RNR and elevation of dATP in cardiomyocytes transduced *in vivo*. Targeted delivery of DNA for

therapeutic use has been a goal for decades, and the first virally-mediated gene therapies have recently been approved in both the US and Europe (35, 36). These therapies use replication-defective adeno-associated viruses (AAVs) to deliver cDNA which will only be encoded by specific cell types based on specially selected and designed promotor regions of the genes. Despite many attempts, there has not yet been a successful trial of cardiac gene therapy in humans. The most high-profile case thus far has been the CUPID (Calcium Upregulation by Percutaneous administration of gene therapy In cardiac Disease) trial, which used an AAV1 to induce targeted overexpression of SERCA2a in the myocardium of patients experiencing heart failure(37–39). Despite promising results from early stages and demonstration of safety, CUPID was suspended when Phase IIb results failed to show therapeutic efficacy. The authors concluded that this was largely due to low transduction efficiency (40, 41).

There are still many hurdles to clear before cardiac gene therapies will be viable. Particularly difficult is balancing efficiency of delivery with tissue specificity. There are many variables that must be considered when designing a vector: viral serotype, the gene to be delivered, the promotor region, and required viral titer. First and foremost, the treatment must be effective in a dose that will not elicit an immune response. Different serotypes of AAV have variations in capsid proteins that result in differential affinity for transducing different tissues as well as different antibodies during immune response. Patients must be pre-screened for antibodies to the desired serotype to minimize risk of adverse reactions. The promotor should be a sequence specific to the target tissue (such as hematopoietic cells, motor neurons, or cardiomyocytes). Finally, gene chosen should encode a protein whose increased expression will alleviate or compensate for the specific pathology that is also small enough to be contained within an AAV's relatively small packing capacity of approximately 4,500 base pairs.

Our group has made significant progress in developing promotors for gene therapies which can target cardiac muscle specifically using a promotor modified from cardiac troponin T (2, 42) or both cardiac and skeletal muscle using a promotor derived from a creatine kinase gene (CK8). RNR-based gene therapy is unique in that the therapeutic element is not the protein itself but the nucleotide, which is able to diffuse freely between transduced and non-transduced cells (5), which we postulate can compensate for incomplete viral transduction better than a protein which needs to be overexpressed in every cell for therapeutic effect.

Chapter 2. CARDIAC MYOSIN ACTIVATION WITH 2-DEOXY-ATP VIA INCREASED ELECTROSTATIC INTERACTIONS WITH ACTIN

Powers, JD, CC Yuan, KJ McCabe, JD Murray, MC Childers, GV Flint, F Moussavi-Harami, S Mohran, R Castillo, C Zuzek, W Ma, V Daggett, AD McCulloch, TC Irving, M Regnier. 2019. Cardiac myosin activation with 2-deoxy-ATP via increased electrostatic interactions with actin. *Proceedings of the National Academy of Sciences* 116 (23):11502-11507.

2.1 INTRODUCTION

Heart failure (HF) is a chronic progressive condition in which the heart is unable to efficiently pump blood through the body, and it is a significant and growing medical challenge. Current treatments only slow progression of HF and do not rescue cardiac muscle function. Consequently, there is a pressing need for novel therapeutic interventions that enhance cardiac contractility in failing hearts.

Cardiac muscle generates force through cyclical ATP-driven interactions between actin and myosin, making myosin an appealing target for treating ventricular systolic dysfunction. Several small molecules targeting myosin are in development for treatment of HF; one is the naturally occurring ATP analogue 2-deoxy-ATP (dATP). The Regnier Lab has previously demonstrated that dATP can be used by cardiac myosin in place of ATP as the substrate that fuels actin-myosin cross-bridge cycling (43). Moreover, we have shown that dATP increases contractility in rat myocardium (43), improves left ventricular function in a porcine model of myocardial infarction (3), and increases contractility of ventricular muscle from patients in human end-stage heart failure (1).

Chemo-mechanical studies suggest that the dATP-mediated force augmentation occurs by increasing cross-bridge binding and cycling rates (30–32, 44), but a precise structural explanation for this is lacking. A recent computational study using molecular dynamics simulations suggests that dATP behaves as an allosteric effector of pre-powerstroke myosin, such that when dADP.P_i is in the nucleotide binding pocket, local structural changes lead to exposure of more positively charged residues on the actin binding surface of myosin compared with ADP.P_i (6). This led us to hypothesize that dATP increases electrostatic interactions between cardiac myosin and actin,

which should result in a destabilization of the resting conformation of myosin in the cardiac sarcomere and prime myosin for binding to actin to increase cross-bridge formation during activation.

Assessing how small changes in myosin structure translate to large changes in sarcomere dynamics, contractility, and cardiac output is a challenge that requires a combination of techniques that span multiple spatiotemporal scales. To test these hypotheses we have developed a novel, multidisciplinary approach to investigate the mechanisms of action of a specific inotropic agent (dATP) with potential therapeutic applications in cardiac muscle that incorporates anatomically detailed analysis of molecular structure, Brownian dynamics simulations of actin-myosin binding kinetics, and small-angle X-ray diffraction analysis of sarcomere structure. Specifically, atomistic structural models of pre-powerstroke myosin-ADP, myosin-dADP, and actin were used to investigate how the change in nucleotide affects the steric orientation of the actin-myosin binding surface and the energetics associated with the actin-myosin complex. Brownian dynamics (BD) simulations [using Browndye software (45)] of myosin binding to an actin dimer with either ADP or dADP suggest that dADP-myosin has an increased number of polar residue interactions between the actin-myosin interface compared to ADP-myosin, which is predicted to increase the association kinetics. Next, F-actin filament binding on cardiac myosin-coated surfaces in solutions of varying ionic strength was used to experimentally confirm the role of surface charge on actin-myosin binding with ATP vs. dATP. Finally, the results of the x-ray diffraction studies suggest that dATP alters the resting conformation of myosin in the sarcomere, facilitating the movement of the S1 head away from the thick filament backbone and towards actin. Lowering ionic strength of the solution (thereby increasing the surface charge of the proteins) reduced the advantage of dATP in facilitating myosin movement, supporting the hypothesis that dATP-induced structural changes in myosin promote myosin-actin interaction via increased electrostatic contacts. Moreover, meridional x-ray diffraction patterns indicated that the resting (pCa 9.0) myofilament structure with dATP closely resembles a submaximal active state with dATP. Moreover, meridional X-ray diffraction patterns indicated that the resting (pCa 9.0) myofilament structure with dATP closely resembles a submaximal active state with ATP. Taken together, our novel multiscale structural and biochemical analysis that couples computational and experimental methods provides a holistic picture of the mechanisms behind augmented cardiac contractility by dATP and represents a new

framework for characterizing small molecules with potential therapeutic application in ventricular systolic dysfunction.

2.2 METHODS

2.2.1 Animal use and ethics

All animal experiments were done in compliance with protocols approved by both the University of Washington and the Illinois Institute of Technology Institutional Animal Care and Use Committees and followed the "Guide for the Care and Use of Laboratory Animals" (National Research Council, 2011). Fourteen adult male Fischer 344 rats were used in the experiments. The rats were euthanized by carbon dioxide inhalation and exsanguination.

2.2.2 Heart excision and trabeculae preparation

Rat hearts were rapidly excised and perfused via retrograde flow through the aorta with room-temperature and oxygenated (95% O2 and 5% CO2) Krebs-Henseleit (KH) solutions containing (in mM) 118.5 NaCl, 5 KCl, 1.2 $MgSO_4$, 2 NaH_2PO_4, 25 $NaHCO_3$, 1.8 $CaCl_2$, 10 glucose, and 20 2,3-butanedione monoxime, (BDM; used to minimize damage during dissection). Papillary muscles and trabeculae were carefully dissected from the right ventricle and immediately placed in 'skinning' solution containing 100 mM KCl, 10 mM MOPS, 5 mM EGTA, 9 mM $MgCl_2$ and either 1 mM dATP or 4 mM ATP (adjusted to pH = 7 with KOH), 1% (by volume) Triton X-100 and 1% protease inhibitor (Sigma P8340) at room temperature. The solution was replaced every 30-45 minutes and preparations were removed after 90-120 minutes of incubation in the skinning solution. Custom aluminum T-clips were placed on each end of the preparations to facilitate mounting them between a rigid post and a dual-action length/force transducer (Aurora Scientific 402A). Skinned muscle preparations were then washed 3 times with solution without TritonX-100 on ice. Skinned muscles were transferred to 'resting solution' (pCa 9.0) containing either 2mM dATP or ATP before X-ray experiments. Preparations were only ever in contact with ATP or dATP-containing solution once skinning had begun.

2.2.3 X-ray diffraction of skinned cardiac muscle

X-ray diffraction experiments used the small-angle instrument on the BioCAT beamline 18ID at the Advanced Photon Source, Argonne National Laboratory(46). X-ray focal spots were about 0.5 x 0.5 mm at the sample and 0.06 x 0.15 mm at the detector with a maximum incident flux of 10^{13} keV photons/s. To reduce radiation damage, the beam was attenuated (typically 10-fold) using aluminum attenuators. The sample-to-detector distance was 3 meters. Skinned muscle preparations were mounted in a custom mechanics rig allowing for simultaneous X-ray diffraction and mechanics measurements. Fibers were mounted on a 500 mV force transducer (Model 402A, Aurora Scientific Inc.) and force was monitored by an ASI 610A data acquisition and control system. Solutions were changed using a syringe pump equipped with a multiway valve (Hamilton model 500). Sarcomere length was adjusted to ~2.0 μm using laser diffraction (or by adjusting the length such that the trabeculae is taut) and stretched by 15% to reach a length of 2.3 μm. Simultaneous force and diffraction pattern measurements were performed in pCa 9.0 and pCa 5.2 solutions. Diffraction patterns were collected only at the plateau phase of force development in activation pCa 5.2 solution. Small-angle X-ray diffraction patterns were collected on a CCD-based X-ray detector (Mar 165, Rayonix Inc. Evanston, IL). The instrument was calibrated using the 58.380 d_{001} peak of a silver behenate standard.

2.2.4 X-ray data analysis and statistics

The data were analyzed using data analysis programs belonging to the MuscleX software package (Version 1.13) developed at BioCAT (47). The lattice spacing and intensity ratios were measured using the "Equator" routine in MuscleX. The spacing and intensity of the M3 layer were measured using the "Diffraction Centroids" routine in MuscleX. The M3 intensity has been normalized with the total intensity of the estimated diffuse background generated by the "Quadrant fold" routine.

2.2.5 Brownian Dynamics Simulation

Simulations were performed using Browndye software to determine the differences between ATP- and dATP-bound myosin in terms of actin association (45). A previous Molecular Dynamics study on pre-powerstroke myosin (PDB: 1VOM) yielded the starting structures for our myosin rigid bodies(6). PDB files for Run 1 of the MD simulations at the 50,000 ps timepoint with only protein

present (no ligands) were used for both ADP-bound and dADP-bound myosin. An actin monomer (PDB: 2ZWH) with all ligands removed was used to represent the thin filament to avoid electrostatic interactions with other binding sites along the filament. The actin and myosin-ADP structures were manually aligned using Visual Molecular Dynamics (VMD) to ensure that the myosin binding cleft on actin was appropriately oriented with the binding domain on myosin. To ensure the accuracy of the bound conformation, the actin monomer was aligned with Chain B of PDB:5KG8 (rigor myosin X co-complexed with actin) and the myosin structures were aligned with chain A of the same PDB structure. The dADP-myosin and ADP-myosin structures were aligned to an identical structure using VMD to ensure that the simulations are fully comparable.

PQR files were generated for all structures using PDB2PQR (48). Electrostatic potential grids were generated using APBS version 1.4 by solving the Poisson-Boltzmann equation using the Amber force field at 300K(49). A relative permittivity of 4 was used for the solute, and 78.5 for the solvent, and a 0.15 mM concentration of KCl was assumed for the system. A list of polar complex pairs (defined as 'contact pairs') was generated by comparing the myosin and actin input coordinates and considering pairs of atoms within 3.5 Å of each other, and the complete list of contact pairs can be found in associated files. A total of 49 atom pairs met the criteria for the ADP case, and 66 atom pairs met the criteria for the dADP case. A simulation trajectory was considered successful when at least 3 polar contact pairs were within the prescribed 'reaction distance' criterion, and association rates were determined by using the ratio of successful to unsuccessful trajectories together with the assumed diffusivity of the molecules (50). The reaction distance criterion was varied to examine a large range of possible rates since experimental association rate data for this system are unavailable. One million trajectories were performed to calculate the average association rates for both the ADP and dADP case.

2.2.6 In-vitro motility assay

In-vitro motility (IVM) assays were performed as previously described (51). In brief, cardiac myosin was prepared from male Fischer 344 rat ventricles by first adding extraction buffer (0.3mM KCl, 0.15mM Imidazole, 10mM $Na_2P_2O_7$, 1mM $MgCl_2$, 2mM DTT) to minced ventricle tissue and stirring for approximately 30 minutes in a small beaker. Excess protein and residual actin were then removed by centrifugation for 1 hour with the supernatant then diluted in 2 mM DTT on ice

for 1 hour to allow for myosin precipitation. Heavy meromyosin (HMM) and Rhodamine-phalloidin– (RhPh; Molecular Probes, Eugene, OR) labeled F-actin was prepared from rabbit skeletal muscle as described by Kron and colleagues (52). Harvested HMM was stored in -80°C for up to a week with 1% sucrose and 1% protease inhibitor (Sigma-Aldrich, St. Louis, MO). F-actin was prepared from rabbit skeletal muscle ether powder-labelled with rhodamine-phalloidin (Invitrogen, USA) as previously described (52–54) and stored at 4°C for up to 6 weeks.

Flow cells were constructed from two glass cover slips separated by 2-mm foam adhesion strips with a total chamber volume of ~60 µL. The lower side surface was coated with 0.1% nitrocellulose in amyl-acetate (Sigma). Experimental procedure was similar to Gordon and colleagues (55). Briefly, isolated HMM (0.16 mM) in Buffer D solution (2mM $MgCl_2$, 5mM EGTA, 5mM DTT, 10mM Imidazole, 0.2mM PMSF) was added to the flow cell for 3 minutes followed by bovine serum albumin (0.5mg/mL BSA) in actin buffer (AB) (50mM Imidazole, 2mM EGTA, 8mM MgCl2, 50mM KCl) to block nonspecific protein binding to the surface. This was then followed by an AB wash, addition of non-labeled sheared F-actin (1 µM) for 1 min, followed by another AB wash, and finally the addition of 0.5mM ATP in AB. This was followed by another AB wash and RhPh F-actin was then added for 1 minute, finally followed by the experimental motility buffer (MB) with varying ionic strength. Percent composition of MB was 50% AB, 0.04% 1mM DTT, 0.06% Cocktail solution (0.3M Catalase, 1.66M Gl. Oxidase, 50M D- glucose) 2mM ATP/dATP, and 2M KCL). Variation in ionic strength depended on volume percentage of 2M KCL, with 0% at IS 50 and linearly increasing by 0.005% per 10mM of IS. The motility buffer was then heated to 30°C on the slide for approximately 3 to 4 minutes. Each experimental slide was analyzed in at least six different regions, with the recording set for 10 seconds, each at 10Hz with IVM Image Acquisition. Recordings were then analyzed digitally, using a custom software developed by our laboratory that allows for filament counting and tracking.

2.3 RESULTS

2.3.1 Electrostatic restructuring of the actin-myosin interface via dADP.P_i leads to increased binding kinetics

In pre-powerstroke myosin, dADP.P_i allosterically affects myosin, resulting in a structural rearrangement of the nucleotide binding pocket that translates to an altered actin-binding region

of myosin(6). However, the effects of the altered actin-binding region of myosin by dADP.P_i on the actin-myosin association kinetics remained unknown. Here, we used atomically detailed structural representations of actin and myosin to investigate how either dADP.P_i or ADP.P_i (represented as dADP or ADP hereafter) bound to pre-powerstroke myosin affects the steric orientation and alignment of the actin -myosin interface, the electrostatic potential of the actin-myosin complex, and the actin-myosin binding kinetics. Figure 2.1A shows the bound conformation of the actin-myosin complex with myosin-ADP in red, myosin-dADP in blue, and an actin monomer in green. With dADP bound to myosin, there is a significant increase in the number of residue "contact pairs" defined as being < 3.5 Å apart) compared to myosin-ADP (66 pairs for dADP compared to 49 for the ADP case). Figure 2.1B depicts the various residue interactions for actin and the actin-binding surface of myosin-ADP (black lines) or myosin-dADP (blue lines), where the thickness of the lines corresponds to the number of atoms in 'contact' between the two residues. The diagram highlights the increased actin-myosin interactions in the dADP case via the myosin polar residues ASN541, LYS546, HIS548 and HIS550, and SER549 and SER552. Moreover, for myosin-dADP, more atomic contact pairs are associated with serine, lysine, and histidine (Figure 2.1C).

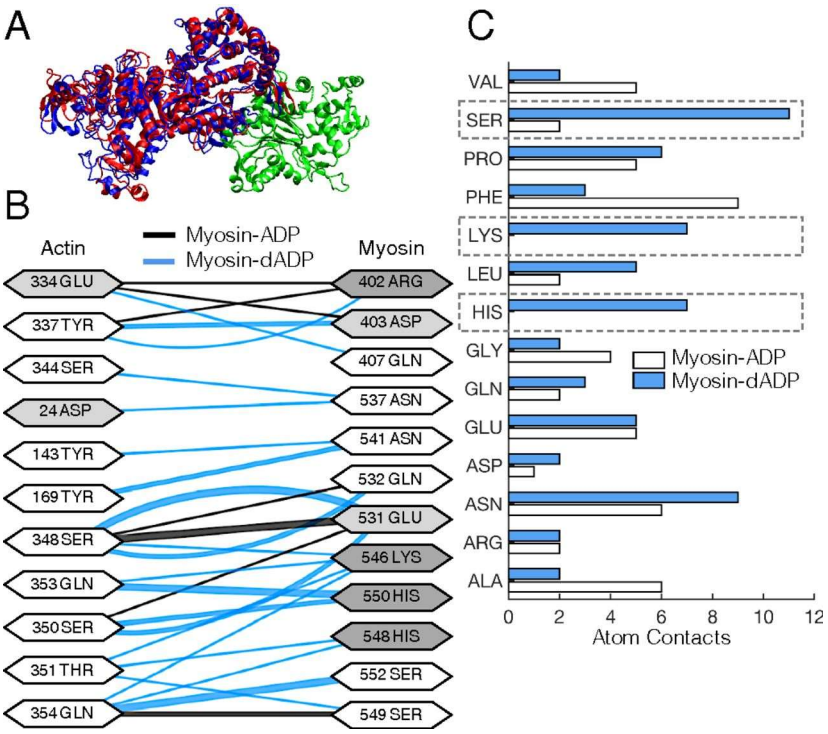

Figure 2.1. dADP acts as an allosteric myosin effector to promote polar interactions between actin and pre-powerstroke myosin. (A) Actin monomer (green) and either ADP-bound (red) or dADP-bound (blue) myosin S1 segments. (B) Contact pairs of residues between actin and ADP-bound myosin (black lines) and dADP-bound myosin (blue lines) for an actin-myosin complex. The thickness of the line connecting the interacting residues corresponds to the number of atoms in contact between the residues, and the shading of the residue indicates whether it is polar (white), acidic (light gray), or basic (dark gray). (C) Number of atoms in "contact" (discussed in the text) between actin and myosin-ADP (white bars) and myosin-dADP (blue bars) in a pre-powerstroke actin-myosin protein complex. There are significant increases in atom contacts that consist of polar residues (SER, LYS, and HIS; highlighted by dashed boxes) between actin and myosin-dADP compared with actin and myosin-ADP.

Bringing more polar residues on myosin into the actin-myosin interaction likely increases the number of hydrogen bonds between myosin and actin, leading to a more stable complex formation. Consistent with this, upon calculating the electrostatic potential (free energy) of the actin-myosin complex for each nucleotide case, we found that the electrostatic potential associated with the actin-myosin protein complex is approximately 8% lower with dADP bound to myosin compared to ADP (-3.21×10^4 kcal·mol^{-1} versus -2.96×10^4 kcal·mol^{-1}, respectively). Thus, our computational

structural analysis (combined with our previous study) predicts that dADP acts as an allosteric myosin effector to directly increase the number of polar interactions between actin and myosin, thereby increasing the electrostatic affinity of myosin for actin. Specifically, we propose that interactions formed by ADP and dADP within the nucleotide binding pocket allosterically result in distinct actin-binding site conformations by altering the dynamics of the switch 1 loop.

Table 2.1 Second-order bimolecular association rate constants for myosin-ADP or myosin-dADP binding with an actin dimer. Rate constants were determined by BD simulations, as described in the text and SI Appendix. For each nucleotide, as the reaction distance criteria decreases, the on-rate increases nonlinearly. However, the on-rate for dADP-myosin to the actin dimer is consistently greater compared with ADP-myosin for all reaction distance criteria, with the greatest fold change in the range of 1.2–2.5 nm. This strongly supports the notion of an increased electrostatic affinity between actin and myosin induced by dADP.

Reaction distance criteria, nm	Actin-myosin on-rates, μM−1·s−1		
	Myosin-ADP	Myosin-dADP	Fold change
0.7	0.42	0.82	1.9
0.8	1.66	4.18	2.5
1.0	8.02	22.02	2.7
1.2	21.37	76.84	3.6
2.5	403.10	1431.73	3.6
5.0	3,198.05	4,460.93	1.4

Based on these results, we hypothesized that increased electrostatic interactions between actin and myosin-dADP will increase the actin-myosin association kinetics. However, given the extremely rapid kinetics of weak crossbridge binding, it is very difficult to measure the associated rates experimentally. Thus, we employed a robust set of Brownian dynamics (BD) simulations to estimate 2nd order bi-molecular associate rates for the actin-myosin complex with either dADP or ADP bound in the nucleotide binding pocket of myosin. Association rates between actin and ADP-bound or dADP-bound myosin were determined for a wide range of "reaction distance" criteria, defined as the minimum separation distance between specified atomic contact pairs in the actin-myosin complex required to reach before a reaction was considered to have occurred. We

simulated binding of myosin to an actin dimer (500,000 independent trajectories) rather than an actin monomer (as shown in Figure 2.1 to provide a more realistic landscape of myosin finding with F-actin while maintaining computational efficiency. Intuitively, association rates are predicted to increase with increased 'reaction distance' criteria for either nucleotide (Table 2.1). Furthermore, as we hypothesized, myosin-dADP is predicted to have a higher association rate with actin compared to myosin-ADP, with the greatest fold-change occurring in the range of reaction distance criteria of 1.2 to 2.5 nm. This is likely due to the allosteric response of pre-powerstroke myosin bound to dADP that leads to a more positively charged binding surface of myosin-dADP in the loop 2 region (6) and increased polar hydrogen bonding interactions (Figure 2.1), which together contribute to a greater electrostatic affinity between actin and myosin and faster association kinetics.

2.3.2 dATP promotes electrostatic interaction of unregulated actin filaments and cardiac myosin in vitro

To experimentally test the hypothesis that dATP promotes electrostatic actin-myosin association (based on the predictions of our BD simulations), we used the *in vitro* motility (IVM) assay. This assay allows the study of actin-myosin interactions and how they are affected by changing conditions (ionic strength, temperature, pH, etc.). In many studies, the ionic strength of motility solutions is maintained between 40 to 100 mM because ionic strength of near-physiological conditions (~170 mM) tend to disrupt electrostatic interactions, resulting in dissociation of actin from myosin coated surfaces and floating away from the plane of focus(56, 57). Previous work using IVM assays with heavy meromyosin (HMM) from skeletal muscle demonstrated that as ionic strength was increased (above ~100 mM), the fraction of motile actin filaments indeed decreased due to weakened electrostatic interactions with myosin, but the reduction was lessened with dATP (6). Because the polar and charge-based surface map differs somewhat between cardiac myosin and fast skeletal muscle myosin, it was important to establish whether dATP has a similar effect with the cardiac myosin in the current work. We hypothesized that cardiac HMM would also maintain a higher degree of actin filament interaction with dATP as ionic strength increases. This is demonstrated in Figure 2.2, showing a greater fraction of F-actin interaction (sliding) as ionic strength is increased up to 130 mM. Greater consistency of electrostatic interactions resulted in significantly increased F-actin filament sliding velocity across a wide range

of ionic strengths (Figure 2.2A). Increased sliding velocity and NTPase rate with dATP has been reported in previous work (43), but we demonstrate here that dATP significantly increases the interaction between actin and cardiac myosin across a wide range of ionic strength compared to ATP. This further supports the notion that dATP enhances the electrostatic interaction between actin and cardiac myosin relative to ATP.

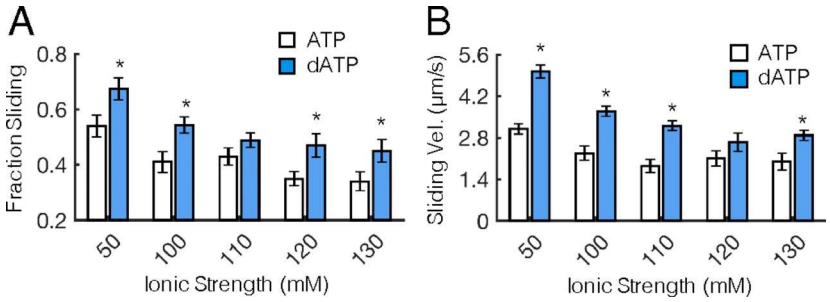

Figure 2.2. dATP promotes motility of unregulated F-actin across a range of ionic strengths. (A) Fraction of sliding actin filaments is significantly greater across a range of ionic strengths for dATP-bound myosin (blue bars) compared with ATP-bound myosin (white bars). (B) (Nonerratic) filament sliding velocity (Vel.) is also significantly increased across a wide range of ionic strengths for dATP compared with ATP, likely owing to a combination of increased ATPase rates and increased actin affinity of dATP-bound myosin compared with ATP. *$p < 0.05$ with an unpaired Student's t test. Error bars represent SEM for $n \geq 12$ slides.

2.3.3 dATP alters the resting structure of myosin in the sarcomere

To experimentally determine how dATP affects the structure and proximity of myosin to actin within the sarcomere, we used small-angle x-ray diffraction of chemically demembranated (skinned) rat cardiac muscle preparations. Trabeculae or papillary muscles were skinned in relaxing solutions containing either ATP or dATP and maintained in the same nucleotide species throughout the entire experiment. Measurements were made in physiological (170 mM) and low (100 mM) ionic strength solutions at sarcomere lengths (SL) 2.0 and 2.3. To determine if dATP promotes electrostatic actin-myosin association we used the *in-vitro* motility (IVM) assay. It is important to note that 100 mM is considered a low ionic strength in this experimental assay (contrasted to IVM, where 100 mM is relatively high) and has been used to alter the actin-myosin interaction sarcomere lattice geometry in previous work (58, 59).

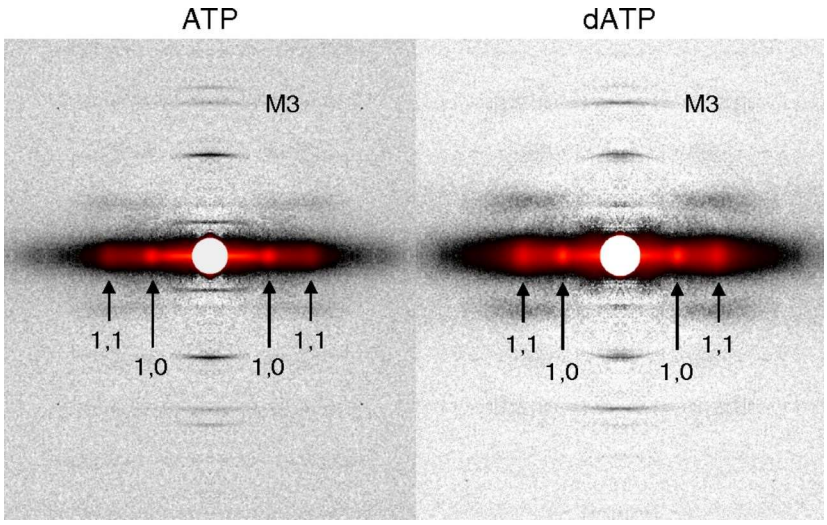

Figure 2.3. Sample X-ray diffraction patterns of resting cardiac muscle. Demembranated cardiac trabeculae or papillary muscles from rat right ventricles were exposed to the X-ray beam while bathed in solutions containing ATP (Left) or dATP (Right) (pCa 9.0, ionic strength = 170 mM, SL = 2.3 μm). In each diffraction pattern, the reflections of interest are labeled. M3, myosin-based meridional reflection due to the axial repeat of myosin crowns; 1,1 and 1,0, equatorial reflections due to the planes of symmetry in the cross-section of the myofilament lattice.

Figure 2.3 shows sample 2D X-ray diffraction patterns of resting (pCa 9.0) permeabilized cardiac preparations in ATP or dATP solutions (ionic strength 170 mM). From these images, we can quantify: (*i*) the intensity and spacing of the myosin-based meridional reflection (I_{M3} and S_{M3}, respectively), which correspond to the periodicity and axial separation distance (respectively) of myosin heads along the thick filament, (*ii*) the filament lattice spacing by measuring the spacing of the 1,0 reflection ($d_{1,0}$) in the equatorial axis, and (*iii*) the ratio of the intensities of the 1,1 and 1,0 equatorial reflections ($I_{1,1}/I_{1,0}$) as an indicator of the radial distribution of myosin mass relative to the thin and thick filaments.

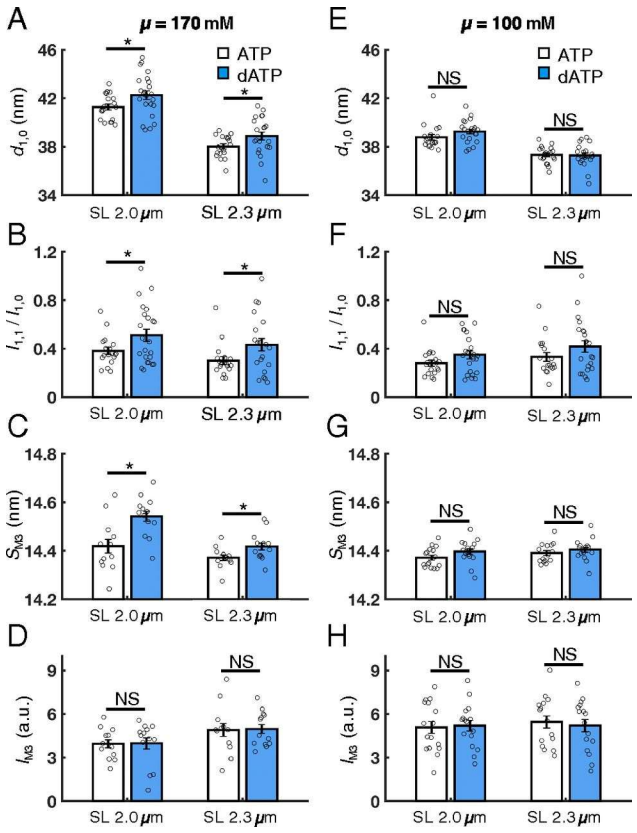

Figure 2.4. Effects of dATP on lattice geometry and myofilament structure in resting cardiac muscle (pCa 9.0). At physiological ionic strength (μ = 170 mM), dATP (blue bars) significantly increases the lattice spacing (A, $d_{1,0}$), the intensity ratio of the primary equatorial reflections (B, $I_{1,1}/I_{1,0}$), and the spacing of the M3 reflection (C, S_{M3}) at both short and long SLs compared with ATP (white bars), but does not affect the intensity of the M3 reflection (D, I_{M3}) at either SL. However, at low ionic strength (μ = 100 mM), these effects are diminished at both short and long SLs (E–G) and the I_{M3} remains unaffected by dATP (H). Error bars represent SEM for n ≥ 14 preparations. *p < 0.05. a.u., arbitrary units; NS, not significant.

Under physiological ionic strength conditions, in the absence of calcium (pCa 9.0), cardiac muscle with dATP had significantly increased inter-filament lattice spacing ($d_{1,0}$) compared to ATP at both short and long SL (Figure 2.4A). Interestingly, the $I_{1,1}/I_{1,0}$ intensity ratio was also significantly increased at both SLs (Figure 2.4B). This suggests that dATP causes a shift in the distribution of the mass of the myosin heads away from the thick filament backbone and toward the thin filament.

We then investigated the effects of nucleotide on myosin filament structure by examining the myosin-based meridional X-ray reflections. Cardiac muscle with dATP had a significantly increased S_{M3} compared with ATP-treated muscle at both SL and μ = 170 mM (Fig. 4C), while the I_{M3} did not significantly differ with nucleotide species at either SL (Fig. 4D). This suggests that the average axial separation of the myosin heads (*i.e.*, distance along the thick filament backbone) is increased with dATP compared to ATP, but the degree of axial ordering of the myosin heads was not affected.

Next, because it has been shown previously that reducing the ionic strength of the solution intrinsically increases the affinity of myosin for actin(58), we hypothesized that if the effects of dATP observed at physiological ionic strength on myofilament structure are electrostatic in nature (as suggested by our simulation and IVM data), then lowering the ionic strength would diminish these effects such that sarcomere structure would be similar to that with ATP. Indeed, there were no significant differences between cardiac muscle with dATP versus ATP in any of the X-ray reflections investigated at low ionic strength (100 mM), at either SL (Figure 2.5). Moreover, these parameters are insensitive to changes in SL at either ionic strength.

Thus, our structural data collected in relaxed (pCa 9.0) cardiac muscle preparations demonstrate that, compared to ATP, dATP alters the resting conformation of myosin heads on the thick filament backbone, causing them to be positioned closer to thin filaments with increased separation distance along the thick filament backbone. Furthermore, the loss of this effect at low ionic strength strongly suggests that the dATP-induced alterations of myofilament structure involve the electrostatic restructuring of myosin predicted by our Brownian dynamics simulations. This conclusion is strengthened by the finding that the effects of dATP on sarcomere and myofilament structure at are unaffected by changes in SL in either ionic strength condition.

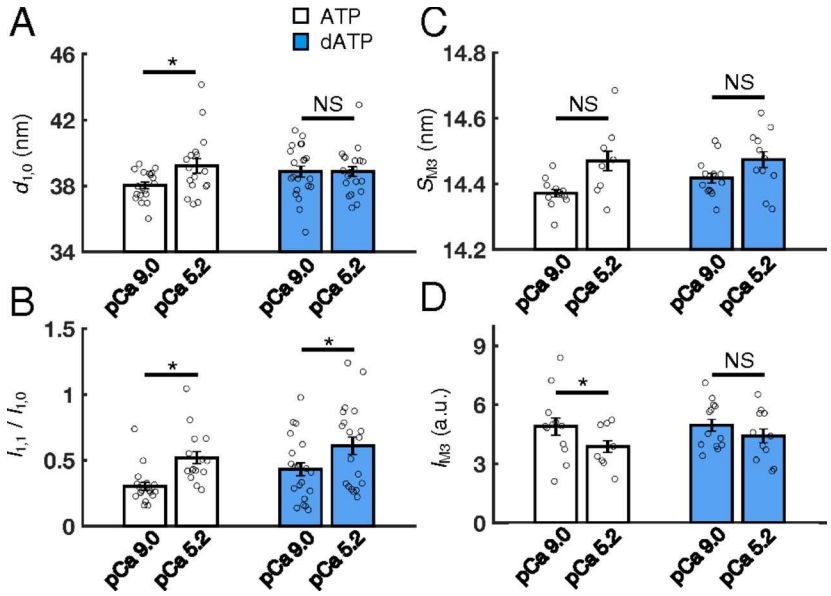

Figure 2.5 Effects of dATP on lattice geometry and myosin filament structure in activated muscle (SL = 2.3 µm, µ = 170 mM). Upon activation (pCa 5.2), cardiac muscle with ATP (white bars) has an increased lattice spacing (A, $d_{1,0}$), an increased $I_{1,1}/I_{1,0}$ ratio (B), no change in the spacing of the M3 reflection (C, s_{M3}), and a significantly reduced intensity of the M3 reflection (D, I_{M3}) compared with resting muscle (pCa 9.0). However, in preparations containing dATP (blue bars), $I_{1,1}/I_{1,0}$ is significantly increased upon activation, while all other parameters are not significantly different between relaxed (pCa 9.0) and activated (pCa 5.2) states. Error bars represent SEM for n ≥ 8 preparations. *p < 0.05 using a paired Student t test. a.u., arbitrary units; NS, not significant.

2.3.4 dATP induces a structural change similar to calcium-mediated activation of thick filaments

Because dATP affects the resting conformation of the of myosin heads in the absence of calcium, it is also possible myofilament structure and lattice geometry may be affected during activation. As such, we compared the myofilament structure between relaxed (pCa 9.0) and sub-maximally activated (pCa 5.2) cardiac muscle with dATP versus ATP at SL = 2.3 µm and ionic strength = 170 mM. Cardiac muscle in ATP had a significantly increased lattice spacing during Ca^{2+} activation, while there were no differences in lattice spacing between resting and Ca^{2+} activated cardiac muscle with dATP (Figure 2.5A). However, the $I_{1,1}/I_{1,0}$ ratio did increase significantly for

both groups during Ca^{2+} activation (Figure 2.5B), indicating that myosin head position relative to actin filaments is similar during isometric contraction. Interestingly, S_{M3} appeared to be moderately increased for both nucleotides during activation at pCa 5.2, but this change was not statistically significant (Figure 2.5C). Finally, I_{M3} was significantly reduced upon cardiac muscle activation with ATP, but not dATP (Figure 2.5D), indicating that the periodicity of thick filaments is less affected during activation with dATP. Thus, dATP has a greater structural effect on cardiac myofilaments at rest than in (submaximally) Ca^{2+} activated muscle.

2.4 DISCUSSION

2.4.1 A structural basis of dATP-mediated force augmentation in cardiac muscle from single molecules to the sarcomere

Our goal in this study was to develop a methodological framework within which we can assess the multiscale mechanisms involved in translating the allosteric effects of small-molecule inotropes on single myosin molecules(6) leading to altered myofilament structure, and ultimately augmented cardiac contractility. Using dATP as our myosin activator, we employed a multifaceted approach that incorporated structural and kinetic information from anatomically-detailed computational simulations with measurements of myofilament structure and sarcomere lattice geometry using x-ray diffraction techniques. Our results suggest that the augmentation of cardiac contractility by dATP is precipitated by structural responses in myosin that later its resting conformation in the sarcomere and increase its electrostatic affinity for actin. Taken together, the novel combination of x-ray diffraction, protein biochemistry, and computational approaches used in this study provide a mechanistic bridge between single-myosin allostery, sarcomere structure, and cardiac contractility.

To summarize, our BD simulations of the bio-molecular association of actin with either ADP-or dADP-bound myosin predict that dADP significantly increases the association rate compared with ADP. We attributed this to a dADP-induced conformational change of the actin-binding surface of myosin that exposes more positively charged and polar residues (Figure 2.1), effectively increasing its electrostatic affinity for actin. We then verified that dATP induces an electrostatic-based enhancement of the actin-myosin interaction by demonstrating an increased fraction of F-actin sliding and increased sliding velocity in the IVM assay with dATP across a wide range of

ionic strengths. Lastly, we used x-ray diffraction analysis to demonstrate that the dATP-induced effects on myosin structure translate into changes in myofilament structure and sarcomere lattice geometry, primarily in resting cardiac muscle. Thus, dATP increases the fraction of myosin motors that are destabilized from the resting conformation compared with ATP, resulting in myosin S1 heads moving closer to actin filaments on average. These changes in resting myosin structure may prime the sarcomere prior to Ca^{2+}-mediated activation, thereby increasing the probability of strong crossbridge formation and cycling.

It is important to note that there are limitations to the simplified BD studies described here. Firstly, the system was assumed to consist of a free-floating myosin S1 head diffusing near a free-floating actin dimer. In the sarcomere the myosin S1 head is tethered to the thick filament, and actin is polymerized into F-actin to form the thin filament, restricting the mobility of each protein relative to one another. The simplifications of the model were chosen to optimize computational efficiency while still elucidating nucleotide-based effects on binding rates. Secondly, enthalpic force calculations included multipole information up to the dipole level as calculated from electrostatic grids using the Adaptive Poisson-Boltzmann Solver (APBS), but the software uses an implicit solvent to maintain computational feasibility which may affect the overall calculation of electrostatic energies. Therefore, the rates we report here should be considered as qualitative (or pseudo-quantitative) evidence for increases in actin-myosin binding due to the presence of dATP rather than exact calculations.

2.4.2 Electrostatic restructuring of myosin by dATP actuates sarcomeres in resting cardiac muscle

Our combined structural and computational data suggest that dATP induces a conformational change in myosin that results in increased exposure of polar and charged amino acid side chains on its actin-binding surface, and that this in turn promotes actin binding when myosin is in the post-hydrolysis, pre-powerstroke state. If the mechanism for the altered resting myofilament structure is mainly increased electrostatic affinity of myosin for actin, then we would expect that compressing the myofilament lattice would enhance these effects by physically bringing actin closer to myosin. This can be done in demembranated muscle by either increasing the osmotic compression with dextran of by increasing SL. Indeed, for pCa 9.0 and μ = 170 mM, $I_{1,1}/I_{1,0}$

increased by 43% at SL 2.3 μm (compressed lattice) for dATP compared with ATP, whereas at SL 2.0 μm (expanded lattice), $I_{1,1}/I_{1,0}$ increased by only 34% (Figure 2.4).

A number of other mechanisms may also contribute to destabilization of the resting state of myosin motors caused by dATP. First, it is possible that the dATP-induced changes in charge distribution of the actin-binding domain my allosterically affect head-head and/or head-tail interactions of resting myosin motors (60). This could be due to a disruption of either the essential light chain-free motor domain interaction, or the blocked motor domain-S2 interaction that has been described in resting skeletal muscle (61). Secondly, it has recently been shown that multiple phosphorylation pathways that target thick filament proteins also affect the resting structure. For example, phosphorylation of myosin-binding protein C (MyBP-C) repositions myosin heads closer to the actin filaments in demembranated cardiac muscle in the absence of calcium (62, 63), while under normal conditions MyBP-C interacts with the S2 domain of myosin and/or the thick filament backbone to stabilize the resting state of thick filaments (64, 65) (20, 21). These findings suggest that MyBP-C plays a significant role in modulating the resting myosin filament structure. It is possible that the change in myosin structure with dATP may alter regulation of the MyBP-C-myosin system in the absence of Ca^{2+}. Furthermore, phosphorylation of the regulatory light chain (RLC) of myosin via myosin light chain kinase (MLCK) also repositions myosin motors closer to actin in resting cardiac muscle (66). This is likely the structural basis of the phosphorylation-dependent increased rate of force development, Ca^{2+} sensitivity of force, and maximum force production in skinned cardiac muscle after treatment with MLCK (66). It is possible that the structural effects of dATP on myosin we present here underpin a similar structural basis of augmented cardiac contractility as these physiological responses.

It has also been demonstrated that systolic force development is regulated by a mechanosensing-based mechanism in the thick filament that occurs downstream from calcium-mediated thin filament activation and involves a rapid feed-forward and load-dependent recruitment of resting myosin motors from strong crossbridge binding (67, 68). In the absence of Ca^{2+} how might the dATP-induced ‘primed’ state of the myosin filament affect such a feed-forward mechanism? The combination of the perturbed resting state of myosin motors and increased electrostatic affinity of actin caused by dATP may work in concert to potentiate cardiac force production both upstream and downstream of Ca^{2+}-mediated thin filament activation by increasing the fraction of ‘actuated’

motors (*i.e.* motors that are positioned closer to actin and primed for strong crossbridge formation) in the absence of Ca^{2+} as well as increasing the probability of strong crossbridge formation and force development upon Ca^{2+}-mediated thin filament activation.

While the focus of this work is not to examine how a dATP-induced enhancement in crossbridge formation may influence thin filament activation, there are some interesting potential implications. For example, given that strongly bound crossbridges can augment azimuthal displacement of tropomyosin on the thin filament (69–71), it is likely that the enhanced crossbridge binding via dATP further amplifies thin filament activation. This is supported by the observation that the slope of steady-state force-pCa curves (indicative of the cooperativity of activation) are not strongly affected by dATP (1). To more directly address this question, high-resolution x-ray diffraction images in future experiments may be able to detect changes in the displacement of tropomyosin with either ATP or dATP as the nucleotide.

2.4.3 Clinical perspectives on targeting the cardiac thick filament

Advances in x-ray diffraction, protein spectroscopy, and electron microscopy have made it possible to gain high resolution structural information of cardiac myosin and thick filament structure. Recent studies utilizing these approaches have primarily investigated the structural consequences of myosin-based mutations associated with cardiomyopathy, as well as small molecule myosin effectors. There are a number of small molecule-based inotropes that target cardiac myosin currently being developed to treat heart failure. One inotrope, omecamtiv mercarbil (OM; also known as CK-1827452 and AMG 423) is currently in phase III clinical trials for treatment of systolic heart failure. OM selectively binds to myosin and increases the fraction of myosin motors that are strongly bound to actin (72, 73) and may increase the transition from weak-to-strong actin-myosin interactions without affecting intracellular Ca^{2+} handling (74). Similar to what we report here for dATP, OM perturbs the regulatory state of the cardiac thick filament and causes myosin motors to switch to a more activated states at low levels of Ca^{2+} where they are more perpendicular to the thick filament backbone (75). Interestingly, despite mobilizing myosin motors in the absence of Ca^{2+}, OM reduces force production at higher Ca^{2+} concentrations in demembranated cardiac muscle while dATP increases force at all levels of Ca^{2+} (44). Therefore, dATP has similar beneficial effects on augmenting systolic pressure development as OM, but in

contrast to OM, systole is not prolonged, and the rate of pressure decline at the end of systole is enhanced (3, 76).

Chapter 3. DEOXY-ATP IN SKELETAL MUSCLE: A PILOT STUDY OF COMBINATORIAL GENE THERAPY FOR DUCHENNE MUSCULAR DYSTROPHY

3.1 INTRODUCTION

In addition to its effect in cardiac muscle, dATP also increases the rate and magnitude of tension development of skeletal muscle at submaximal calcium *in vitro*. It is still unknown whether this shift in calcium sensitivity translates to increased performance *in vivo.* We measured force production in the hindlimb of a transgenic mouse model overexpressing Rrm1 along with a variant isoform of the small subunit of RNR, Rrm2B. These mice have elevated dATP in all tissues measured and represent the theoretical maximum elevation of dATP in muscle tissues. In addition to healthy animals, we also examined the effects of elevated dATP a model of skeletal muscle pathology.

Duchenne muscular dystrophy (DMD) is a genetic disease that affects roughly 1 in every 5,000 boys (77). It is caused by a truncation in dystrophin, a protein that connects the cytoskeleton with the extracellular matrix (ECM) via the dystrophin-glycoprotein complex (DGC). This linkage transduces the force of contraction to the ECM to protect skeletal muscle from contraction-induced injury. The mutation can be either inherited or *de novo*. Ultimately, the absence of dystrophin results in a drastic reduction of all of the DGC components further contributing to membrane destabilization, membrane permeability defects, and myofiber degeneration. The lost muscle is then replaced with fibrosis and adipose tissue. The disease first presents early in life as difficulty moving into a standing position. Over time it progresses to a loss of muscle function and ambulation, respiratory difficulty, and cardiomyopathy. Despite advances in care, average life expectancy for an affected DMD patient is less than 30 years.

Dystrophin is one of the largest known genes, comprising over 2.4 million base pairs. This makes DMD particularly challenging to treat with AAV-mediated gene therapies. Large deletions to dystrophin are also found in the milder Becker muscular dystrophy Several clinical trials have

recently begun using engineered "microdystrophin" constructs which encode limited but functional versions of the protein small enough to package in an AAV capsid (78–80).

The mdx mouse is a model of DMD with a truncation in dystrophin. Despite having a normal mouse lifespan, the model displays abnormal ECG's at 6-months and left ventricular dysfunction at 11-months, closely mimicking the pathological changes in patients with DMD. The major deficiency of the model is that compensatory adaptations occur in limb muscles of *mdx* mice. In contrast, the diaphragm does not exhibit such an adaptation. As such, the diaphragm muscle of the *mdx* mouse more reflects the degenerative changes observed in skeletal muscle of the human DMD condition.

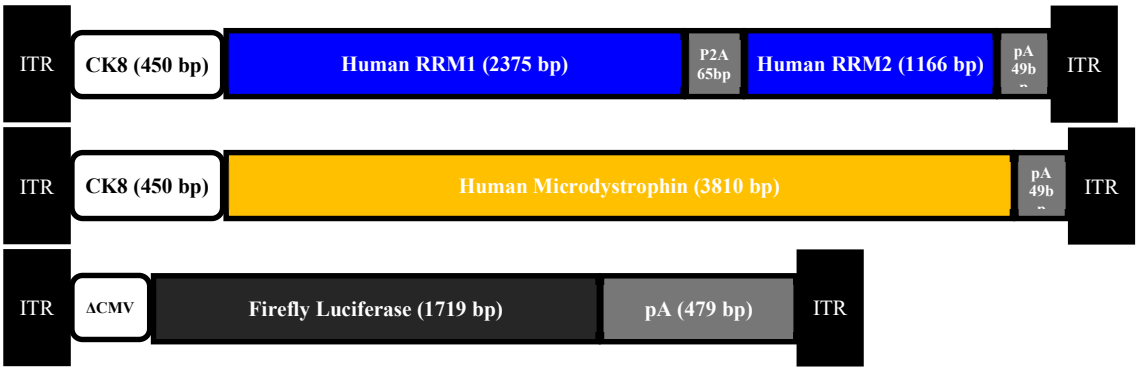

Figure 3.1 Schematic of viral vectors. Single-vector cohorts received an equivalent dose of luciferase control vector to normalize total viral load.

This was a pilot study to test a combinatorial gene therapy for DMD: microdystrophin to address the underlying structural deficiency in the myocytes, and RNR to augment the functional output of the muscle. We therefore developed a viral vector using a CK8 promoter that will deliver RNR to both cardiac and skeletal muscle (AAV6-CK8-RNR), hypothesizing that both cardiac and skeletal muscle will benefit from improved function. We utilized 3 vectors for this study (Figure 1): AAV6-CK8-RNR, an AAV6 encoding a designed microdystrophin also using the CK8 promoter (AAV6-CK8-μDys), and a control vector with a truncated nonfunctional CMV promoter and cDNA for firefly luciferase (CV). We performed functional measurements in both cardiac and skeletal muscle but focused primarily on outcomes in skeletal muscle performance for several reasons. First, during the timeframe of the study (roughly 5 months), mdx mice begin to develop a skeletal muscle phenotype, but cardiac function is not measurably reduced for nearly a year. Additionally, this is the first use of RNR gene therapy utilizing AAV6 with a promotor expressed

in both striated muscle types. The effect of elevated dATP on cardiac muscle has been well characterized, but these are the first *in vivo* measurements of transduced skeletal muscle with elevated dATP.

3.2 METHODS

3.2.1 Transgenic overexpression of ribonucleotide overexpression in mice

The transgenic mice used in this experiment globally overexpressed two subunits of ribonucleotide reductase: the large subunit Rrm1 and the p53-inducible isoform of the small subunit, Rrm2B (81). Tissues from these mice have a tenfold increase dATP content compared to wild-type littermates. Wild-type littermates were used as controls. Results are from males aged 4-7 months unless otherwise noted.

3.2.2 MDX mouse model

All animal experiments were done in compliance with protocols approved by the University of Washington and followed the "Guide for the Care and Use of Laboratory Animals" (National Research Council, 2011). Male mdx4^{CV} mice received retroorbital injections at 14 days of age and were followed for 4 months.

3.2.3 Vector production

rAAV genomes containing the CK8 regulatory cassette (expressed exclusively in skeletal and cardiac muscle) and the human codon optimized (GenScript) mDys (DR2-15/DR18-22/DCT) (24), followed by the rabbit beta-globin polyadenylation (pA) signal, were generated using standard cloning techniques. The rAAV genomes containing the CK8 regulatory cassette, the codon optimized human RNR transgene flanked by 100-bp untranslated regions, and the rabbit beta-globin pA were generated as previously described (48). The "dead" rAAV genomes or promoter-less firefly luciferase followed by the human growth hormone (hGH) pA (kindly provided by J.S.C., University of Washington, Seattle, Washington) were used to generate the control rAAV genomes. The resulting constructs were cotransfected with the pDG6 packaging plasmid into HEK293 cells to generate rAAV vectors carrying serotype 6 capsids, which were harvested, enriched, and quantitated as previously described (49).

3.2.4 Ultrasound measurement of diaphragm function

Diaphragm movement amplitude was measured during regular breathing in anesthetized mice via ultrasonography using a system designed for mouse echocardiography (Vevo 2100, Fujifilm Visual Sonics, Toronto, Canada) as previously described (82).

3.2.5 In vivo *plantar flexion*

Hindlimb skeletal muscle strength was assessed *in vivo* via plantar flexion force-frequency and fatigue protocols using a 1300A 3-in-1 whole animal system (Aurora Scientific, Aurora, ON, Canada). Anaesthetized mice were laid on a heated platform and secured at the knee. One foot was fixed to a foot pedal attached to a force transducer, and subdermal electrodes placed at either end of the gastrocnemius. Muscle contraction was stimulated directly for 200 ms in frequencies ranging from 10 to 200 Hz with a two-minute rest between contractions. To measure fatigue, the muscle was stimulated for 200 ms at 200 Hz with 1 second rests between stimuli for a total of 120 contractions. Further stimulation at 1 minute and 5 minutes post-fatigue measured the force after recovery. Force measurements were then normalized to mass of the gastrocnemius after dissection.

3.2.6 Cardiomyocyte isolation and contractile assessment

Cardiomyocytes were isolated from a subset of mice via enzymatic digestion through retrograde aortic perfusion as described previously. Briefly, hearts were rapidly excised, cannulated, and perfused with a collagenase/protease solution, following which the ventricles were removed, minced, and triturated. Contractile assessments of cells were made immediately after stepwise reintroduction of calcium and incubation in Fura-2-AM to measure calcium transients. Cell shortening and re-lengthening and calcium transients were measured at 37°C using an IonOptix μStep video recording system (IonOptix, Westwood, MA, USA).

3.2.7 dATP quantification in intact muscle

dATP content in soleus muscle was measured by high-performance liquid chromatography-mass spectrometry (HPLC-MS/MS) as described previously5. In brief, soleus muscle samples (~15 mg) were flash-frozen, stored at -80°C and nucleotides were extracted 1-3 days before measurement using a 50% methanol solution. The supernatant was stored at -20°C until ready for injection into

the HPLC-MS/MS system. ATP and dATP standard curves were used to calculate the concentration of each nucleotide. dATP content was then normalized to ATP in the same samples.

3.2.8 Protein analysis

Protein samples were solubilized in 1% NP-40 lysis buffer with 4% protease inhibitors (Sigma) and centrifuged for 14,000 *g* for 5 minutes. The supernatant was mixed with SDS protein sample buffer containing β-mercaptaethanol (Bio-Rad) and resolved by SDS-PAGE on 4-20% Mini-Protean GTX Stain-Free gels (Bio-Rad). Overnight protein transfer to 0.45 mm polyvinylidene difluoride membranes was performed at constant 34 volts at 4°C in Towbin's buffer containing 20% methanol. Blots were blocked for 1 hour at room temperature in 1x BlockerFL (Thermo Scientific) before overnight incubation with primary antibodies raised against the hinge-1 region of dystrophin (Developmental Studies Hybridoma Bank, University of Iowa, 1:300). The same blots were later probed for RNR after overnight incubation in Abcam ab137114 (human Rrm1, 1:1000) and Sigma GW22152A (human Rrm2/Rrm2B, 1:1000).

3.2.9 Statistical analysis

The statistical analyses were performed using GraphPad Prism 8 (Graphpad Software). Comparisons of skeletal muscle function in transgenic mice used Student's t-test. Comparisons of multiple treatment groups in mdx mice were made using one-way ANOVA with Tukey's multiple comparisons. Hindlimb force-frequency relationship was analyzed using two-way ANOVA with Tukey's multiple comparisons. The results shown here are mean ± SEM unless otherwise stated.

3.3 RESULTS

3.3.1 Transgenic overexpression of RNR does not change skeletal muscle strength, but slows relaxation

Unlike cardiac muscle, skeletal muscle is capable of tetanic contraction, a fusion of shorter stimulations without relaxation. We directly stimulated hindlimb plantar flexion muscles of anesthetized mice and measured the torque exerted on a foot pedal. Stimulation frequencies ranged from 10 Hz (single twitches) to 200 Hz. Complete fusion of tetanus occurred at 120 Hz in all animals, and stimulation at higher frequencies does not increase force production. All torque

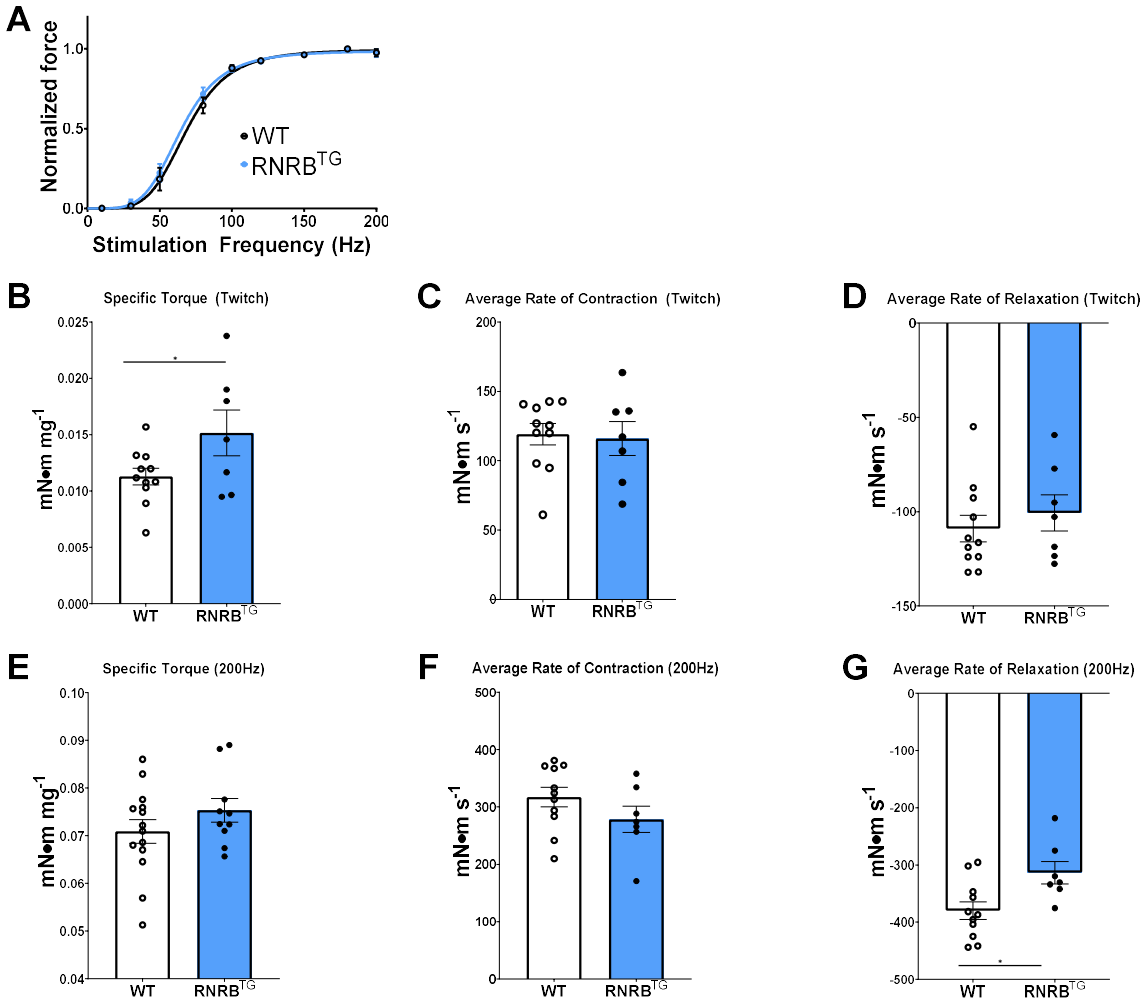

Figure 3.2 *In vivo* hindlimb stimulation of transgenic mice with elevated dATP.

(A) The relationship of stimulation frequency to force production is unchanged in RNRB-TG mice. (B) Transgenic mice generate more twitch force than wild-types when normalized to mass of the gastrocnemius. (C-D) Average rates of twitch contraction and relaxation are unchanged. (E) Maximum stimulated tetanic force and (F) rate of contraction are unchanged in the transgenic mouse, but (G) average rate of post-stimulus relaxation is slowed.

measurements were normalized to the mass of the gastrocnemius, the largest muscle that contributes to plantar flexion. We found no difference in the relationship between force production and stimulation frequency in the hindlimb (Figure 2A). As in the heart, mean specific twitch torque was increased in the transgenic mice with elevated dATP (Figure 2B), which implies that dATP may potentiate contraction in skeletal muscle as it does in cardiac muscle (83). However, the

kinetics of twitch contraction are unchanged (Figure 2C-D) and transgenic mice showed no difference from wild-type in maximum force production or rate of contraction at higher frequencies (Figure 2E-F). Unexpectedly, average rate of relaxation after stimulation is slowed in transgenic mice (Figure 2G). We hypothesize that this may be due to differences in fiber types caused by global overexpression of Rrm1 and Rrm2B during development, but this was not tested.

3.3.2 RNR is only overexpressed in skeletal muscle with the addition of µDys

The CK8 regulatory cassette is expressed in both striated muscle types. To confirm overexpression of RNR and µDys we performed western blot of whole-tissue lysates from gastrocnemius (Figure 4.3A) and cardiac ventricle (4.3B). Microdystrophin was detected in both treatment groups in both muscle types, as was RNR in the heart. Unexpectedly, the mice which received AAV-RNR alone overexpressed both subunits in the heart but not in skeletal muscle. When combined with AAV-µDys, RNR was also present in detectable amounts. We postulate that this is due to increased turnover of skeletal muscle fibers in the mdx mouse leading to complete replacement of the muscle cells over the experimental timeframe which is prevented by introducing the structural support of microdystrophin.

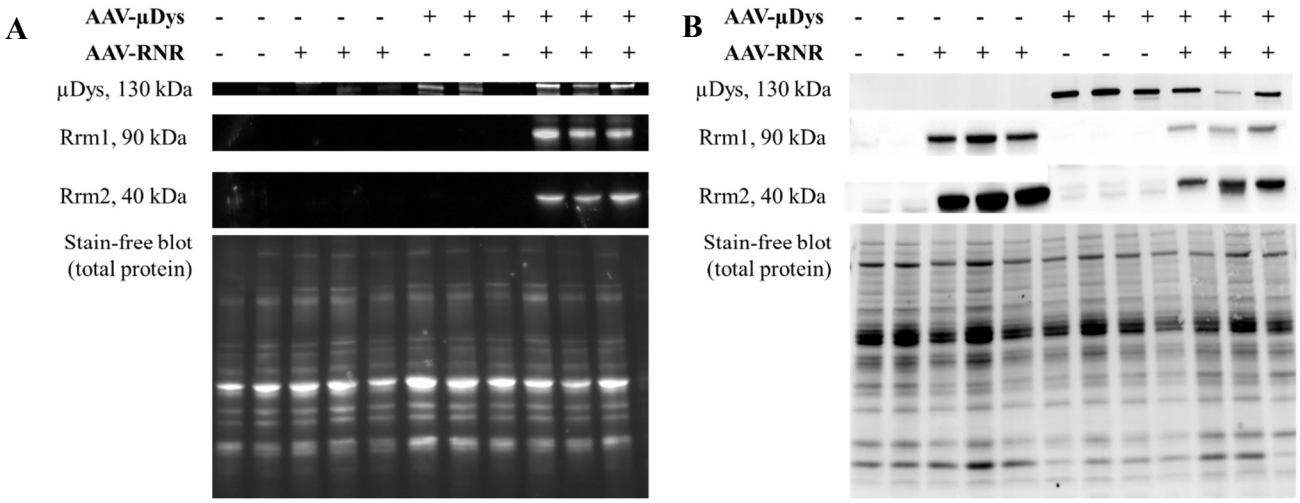

Figure 3.3 RNR and µDys overexpression confirmed by western blot in whole tissue lysates of gastrocnemius (A) and cardiac (B) muscles.

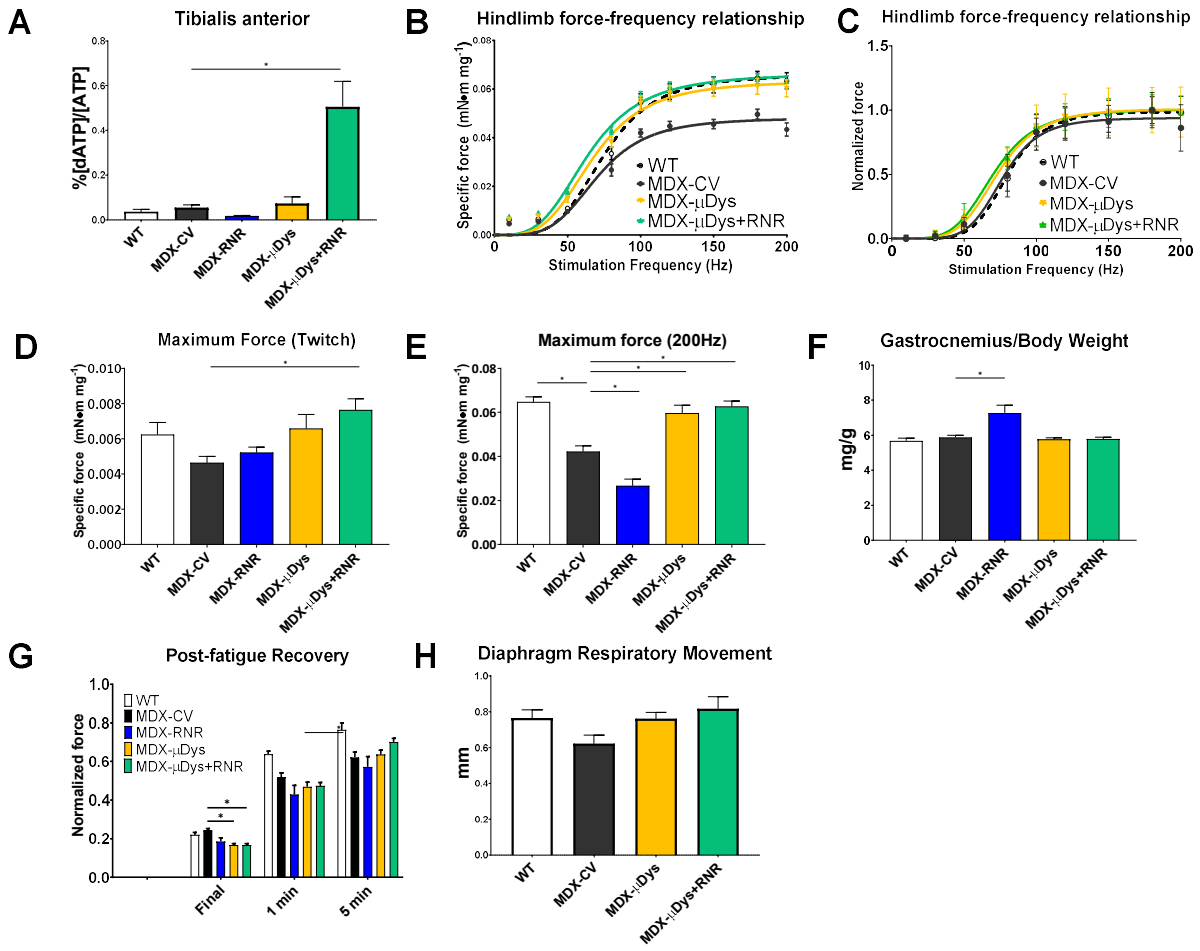

Figure 3.4 Measurements of skeletal muscle function in AAV-treated mdx mice.

(A) Mass spectrometry measurement of dATP content of the tibialis anterior hindlimb muscle, normalized to ATP. Of the two cohorts that received AAV6-CK8-RNR, only the dual-treatment group had elevated dATP. (B-E) *In vivo* measurements of the force production in hindlimb muscles following direct electrical stimulation. There was no difference in force-frequency response between groups. Untreated mdx mice had lower maximum stimulated force compared to WT, which was prevented by treatment with AAV6-CK8-μDys. The addition of RNR did not alter strength or kinetics of the muscle. (F) Mass of the gastrocnemius muscle. MDX mice that received AAV6-CK8-RNR at 2 weeks of age had significant muscle hypertrophy compared to other groups (G) Fatigue resistance and recovery after short rest, normalized to maximum pre-fatigue tetanus. The decreased loss of strength in untreated mice reflects their lower maximum force production before fatigue. (H) Movement of the diaphragm during respiration in anaesthetized mice. We found no significant differences between groups.

3.3.3 Gene therapy improves function and elevates dATP in skeletal muscle

Measurement of dATP levels in the tibialis anterior (TA) muscle follows the trend seen in RNR levels of transduced tissues. The TA was chosen for this assay because it is large enough to provide sufficient tissue for the assay and small enough to homogenize the entire muscle. dATP/ATP was significantly raised with combination treatment but not with RNR alone.

We repeated the hindlimb force-frequency and fatigue protocol on AAV-treated mdx mice four months after injection. A single dose of AAV6-μDys is sufficient to prevent this loss of strength even four months after injection (Figure 3.4). Though the combination group also had elevated dATP/ATP as measured by mass spectrometry, maximum specific forces were not different from the group that received μDys alone. μDys treatment also preserved fatigue resistance in both treatment groups, as post-fatigue tetanic contractions produced more specific force after a five-minute rest. Diaphragm sonography at endpoint showed no change in average movement during breathing, between treatment groups, or between wild-type and untreated mdx mice.

3.3.4 RNR overexpression exacerbates the mdx phenotype

Unexpectedly, the group that received RNR alone did not have elevated dATP in skeletal muscle and displayed an exacerbated dystrophic phenotype. Stimulated hindlimb force was significantly lower than in untreated mdx mice, and gastrocnemius mass was higher with no corresponding change in body mass, meaning specific force was significantly lower. Our suspicion is that without microdystrophin to stabilize new myofibers, increased RNR activity allowed them to grow, degrade, and be replaced by satellite cells until no transduced cells remained at the experiment's endpoint. This hypothesis is supported by the presence of Rrm1 and Rrm2 in Western blots of gastrocnemius samples in from the combination group, but the absence of RNR in the other treatment groups.

3.3.5 RNR treatment enhances cardiac contractility

We isolated cardiomyocytes from a subset of animals and measured contractility and calcium handling during electrical stimulation in unloaded cells. As expected, untreated mdx mice did not have reduced fractional shortening or contractile kinetics compared to wild type (Table 3.1). Somewhat unexpectedly, treatment with microdystrophin alone resulted in a decrease to both. We

hypothesize that this may be due to an increase in cell stiffness in microdystrophin-transduced cells but did not perform experiments to confirm. All measures of cardiomyocyte contractility were rescued in the dual-treatment group compared to microdystrophin alone.

Table 3.1 Contractile and calcium-handling properties of isolated cardiomyocytes.

*$p<0.05$ compared to MDX-μDys. $n\geq34$ cells per group, N = 5 mice per group.

	MDX-CV	**MDX-μDys**	**MDX-μDys+RNR**	**WT**
Baseline SL (μm)	1.82±0.01	1.80±0.01	1.76±0.00*	1.84±0.00
Maximum contraction velocity (μm/s)	-2.90±0.17	-1.98±0.11	-2.54±0.14*	-3.00±0.28
Fractional shortening (%)	9.12±0.50	6.60±0.36	8.60±0.44*	9.50±0.86
Time to peak (ms)	105±3	108±3	113±4	100±3
Maximum relaxation velocity (μm/s)	2.66±0.21	1.57±0.12	2.14±0.13*	2.60±0.29
Time to 50% relaxation (ms)	59±2	68±3	68±5	60±4
Time to 90% relaxation (ms)	120±10	172±12	126±10*	104±6
Baseline calcium (Fura-2 ratio)	1.41±0.02	1.37±0.02	1.48±0.02*	1.25±0.02
Maximum rate of Ca^{2+} release (u/s)	11.90±0.62	9.57±0.65	10.70±0.86	11.55±0.37
Transient increase (ratio units)	0.48±0.02	0.39±0.02	0.44±0.04	0.47±0.02
Increase from baseline (%)	34.30±1.94	29.51±1.88	30.07±2.47	37.54±1.16
Time to peak (ms)	78±2	82±3	83±2	78±2
Maximum rate of Ca^{2+} decay (u/s)	-2.54±0.13	-1.87±0.15	-2.68±0.30	-2.16±0.11
Time to 50% decay (ms)	135±5	149±5	116±4*	174±9
Time to 90% decay (ms)	489±20	519±14	406±17*	631±20

3.4 DISCUSSION

Previous studies of this and other microdystrophin constructs have proven effective at ameliorating the mdx phenotype in skeletal muscle when delivered via adeno-associated viral vectors (42, 79, 84–86). As cardiac function in the mouse model is not significantly impaired until later in life, this pilot study did not focus on possible improvements in contractility either *in vivo* or at a whole-organ level. With that said, other studies in the lab studying aged (>24 months) mdx mice have found a slowing of the maximum rate of relaxation in diastole that was not significantly altered by transduction of microdystrophin but rescued by overexpression of RNR (42).

This pilot study reaffirms the effectiveness of this microdystrophin construct in preserving skeletal muscle function *in vivo*. The addition of RNR did not positively or negatively alter hindlimb strength or fatigue resistance in the cohort which received both vectors, leading us to believe that overexpression of RNR and elevated dATP do not significantly alter skeletal muscle function. This is supported by results from transgenic mice overexpressing Rrm1 and Rrm2B which have elevated dATP in skeletal muscle but no overt differences in their ability to produce force. Unexpectedly, injection of AAV6-CK8-RNR at 2 weeks exacerbated the mdx phenotype, leading to a dramatic decrease in both absolute and specific force production in the hindlimb and hypertrophy of the gastrocnemius. We assume that this is due to increased turnover of muscle fibers that lack the stabilizing influence of dystrophin, as the dual vector group had increased RNR protein measured by western blot but no increase in muscle mass. Additionally, separate studies of this same vector in wild-type mice have seen no increase in muscle mass or hindlimb force production (Regnier lab unpublished data).

Measurements of calcium and contractility in isolated cardiomyocytes suggest that the addition of microdystrophin may increase stiffness and slow relaxation in the sarcomere, as µDys-treated mice had lower fractional shortening along with lower maximum contraction and relaxation velocities and significantly increased time to 90% relaxation. These measures were all rescued in the dual-vector cohort, consistent with other studies of isolated cardiomyocytes with elevated dATP (4, 33). It is important to note that corresponding measures of whole-heart contractility in aged mdx mice do not recapitulate these results (42), suggesting that microdystrophin-dependent changes in

contractility are likely insignificant compared to other factors such as preload, calcium handling, or fibrosis.

3.4.1 Future studies

The experiments described here are a pilot study meant to inform the design of further studies in virally mediated delivery of elevated dATP in models of Duchenne muscular dystrophy in particular and skeletal muscle in general. Unpublished data from our lab suggest that engineered promoters that are expressed in both striated muscle types (cardiac and skeletal) are more effective at gene delivery than the cardiac-specific troponin T promoter used in past studies. Because we are sacrificing specificity for increased expression, it is important to determine what effect elevated RNR has in both healthy and pathogenic skeletal muscle. Results from transgenic and dual-treatment groups are consistent with early studies in skinned (demembranated) skeletal muscle that found no increase in maximum force production when ATP is replaced with dATP and support the hypothesis that, in the absence of underlying pathology, elevated RNR and dATP do not significantly alter skeletal muscle function.

The unexpected finding of increased hypertrophy and dramatically reduced strength and fatigue resistance in mdx mice that only received the RNR vector confirms the importance of these preliminary studies. Based on these results and the lack of elevated dATP in these muscles, we hypothesize that elevating RNR in muscle fibers that are already undergoing damage due to a lack of dystrophin may lead to increased turnover even when compared to the basal mdx condition, resulting in increased hypertrophy and eventually complete replacement of virally-treated muscle fibers. We propose that subsequent experiments of RNR overexpression be performed at a later age, after the initial insult due to dystrophy. Given that the microdystrophin vector (or other means of dystrophin replacement or rescue) will always be necessary to correct the structural deficiencies of this model, it may be that RNR overexpression to augment cardiac function will only be used to rescue a loss of contractility rather than to preserve it.

Chapter 4. OVEREXPRESSION OF RRM2B ENHANCES DATP AND CARDIAC FUNCTION

4.1 INTRODUCTION

Heart failure is a critical reduction in cardiac output, either through reduced pressure development during systole or impaired relaxation during diastole, both of which are dependent on actin-myosin crossbridge cycling. Cardiovascular disease is the leading cause of death worldwide, and its incidence is expected to increase in the near future (87). Treatments for heart failure are therefore an important target for current and future research, and an ideal therapeutic would treat both systolic and diastolic symptoms of cardiac dysfunction.

4.1.1 2-deoxy-ATP directly alters actin-myosin binding

The Regnier lab has repeatedly demonstrated that the addition of the naturally occurring nucleotide 2-deoxy-ATP (dATP) to cardiac muscle preparations enhances the rate and magnitude of both force development and relaxation. Cardiac myosin can bind with dATP in place of ATP, which results in an increase in both the rate and magnitude of tension development and relaxation in a variety of experimental systems in rodent, porcine, canine, and human tissues (1, 5, 29–32) by altering the dynamics of myosin-actin crossbridge formation and increasing myosin recruitment (6). The cytosolic concentration of dATP can be elevated through upregulation of the enzyme ribonucleotide reductase (RNR) (3–5, 32, 33, 43). Left ventricular (LV) heart function and cardiomyocyte contraction are significantly enhanced by raising the level of dATP to only ~1% of the total ATP pool, accomplished by either transgenic or viral (AAV) vector-mediated over-expression of ribonucleotide reductase (RNR; the rate-limiting enzyme in deoxy-nucleotide synthesis). In both mouse and pig models, LV developed pressure and both the rate of pressure development (+dP/dt) and decline (-dP/dt) were increased. If an effective, consistent method of delivery for this enzyme is developed, it could prove to be a valuable treatment for heart failure. Previous work from our lab using transgenic mice demonstrated that mice overexpressing Rrm1 and Rrm2 have elevated cardiac [dATP] and improved systolic function. Virally-induced overexpression of Rrm1 has been stable, in our hands, but we have seen high variability in the

Rrm2 and dATP levels in multiple disease models. Difficulty in stably overexpressing RNR for therapeutic use has spurred our exploration for alternative methods of elevating dATP in the heart.

4.1.2 Structure and regulation of ribonucleotide reductase

Structurally, the functional form of RNR is a heterotetramer with two subunits, themselves being homodimers. The large subunit (Rrm1) contains the catalytic site in which a nucleotide diphosphate (NDP) is reduced to a deoxy-nucleotide diphosphate (dNDP) and a regulatory site by which the enzyme's activity is altered by the relative ratios of ATP and dATP (88, 89). There are two different isoforms of the small subunit encoded by separate genes and regulated by different pathways, designated Rrm2 and Rrm2B. Rrm2 levels fluctuate with the cell cycle in actively dividing cells, reaching a peak in S-phase, after which it is degraded by the ubiquitin-proteasome system. Rrm2B, also known as p53R2, is induced by the tumor-suppressor p53 and has been proposed to be critical for DNA repair, mtDNA synthesis, and mitochondrial homeostasis in nondividing cells (90–92).

Here, we report an animal model overexpressing subunits Rrm1 and Rrm2B (hereafter referred to as RNRB). We hypothesized that RNRB will elevate dATP and improve cardiac contractility in a similar manner to RNR. Indeed, $RNRB^{TG}$ mice have similarly elevated [dATP] in all muscle tissues measured as well as improved systolic and diastolic function measured *in vivo* and *in vitro*. We also found that virally mediated transduction of RNRB to adult cardiomyocytes *in vitro* improves contractile parameters.

4.2 Materials and Methods

All animal experiments were approved by the University of Washington (UW) Animal Care Committee. Animals were cared for in accordance with US National Institutes of Health Policy on Humane Care and Use of Laboratory Animals in the Department of Comparative Medicine at UW.

4.2.1 Transgenic mice

The transgenic mice used in this experiment globally overexpressed two subunits of ribonucleotide reductase: the large subunit Rrm1 and the p53-inducible isoform of the small subunit, Rrm2B (81). Tissues from these mice have a tenfold increase dATP content compared to wild-type littermates.

Wild-type littermates were used as controls. Results are from males and females aged 4-7 months unless otherwise noted.

4.2.2 Echocardiography

Echocardiography was performed on mice at 4 months of age (Vevo 2100, Fujifilm Visual Sonics, Toronto, Canada). LV end-diastolic (LVEDD) and end-systolic (LVESD) dimensions were determined and fractional shortening was calculated using the formula (LVEDD – LVESD)/LVEDDx100. All analysis was done by a single reader.

4.2.3 Isolated perfused mouse heart preparation

Left ventricular contractile kinetics were measured in Langendorff isolated heart preparations as described previously (42). Excised mouse hearts were perfused at a constant pressure of 80 mmHg in a modified Krebs-Henseleit buffer (In mM: 118 NaCl, 25 $NaHCO_3$, 5.3 KCl, 2.0 $CaCl_2$, 1.2 $MgSO_4$, 0.5 EDTA, 5.5 glucose, 0.5 sodium pyruvate, equilibrated with 95% O_2 and 5% CO_2, pH 7.4) at 37°C. After equilibration, baseline function was monitored at a fixed end diastolic pressure of 8-10 mmHg for 10-20 minutes by way of a water-filled balloon inserted into the LV. Balloon volume was increased in 5 μL increments to determine the pressure-volume relationship in the myocardium. Finally, buffer [Ca^{2+}] was increased from 2mM to 4mM for 20 minutes to stimulate an increase in cardiac work.

4.2.4 Adult mouse cardiomyocyte isolation and contractile assessment

Cardiomyocytes were isolated from mice 4-7 months of age via enzymatic digestion through retrograde aortic perfusion as described previously (4). Briefly, hearts were rapidly excised, cannulated, and perfused with a collagenase/protease solution, following which the ventricles were removed, minced, and triturated. Contractile assessments of cells were made immediately after stepwise reintroduction of calcium and incubation in Fura-2-AM to measure calcium transients. Cell shortening and re-lengthening and calcium transients were measured at 1 Hz and 37°C using an IonOptix μStep video recording system (IonOptix, Westwood, MA, USA). Measurements were performed by 4 different experimentalist and analyzed by the same reader.

4.2.5 dATP quantification in cardiac tissue.

dATP content in cardiomyocytes was measured by high-performance liquid chromatography-mass spectrometry (HPLC-MS/MS) as described previously (93). Whole mouse ventricle or isolated cardiomyocytes were flash-frozen, stored at -80°C and nucleotides were extracted 1-3 days before measurement using a 50% methanol solution. The supernatant was stored at -20°C until ready for injection into the HPLC-MS/MS system. ATP and dNTP standard curves were used to calculate the concentration of each nucleotide. dATP content was then normalized to ATP in the same samples.

4.2.6 Mitochondrial respirometry

For mitochondrial respiration experiments, whole ventricles were homogenized on ice for 30 seconds in 5 mL of isolation buffer (210mM sucrose, 2mM EGTA, 40mM NaCl, 30mM HEPES, pH 7.4) and centrifuged for 10 minutes at 900g and 4°C. The supernatant was removed and centrifuged again for 10 minutes at 10,000g and 4°C. The supernatant was discarded and pellet containing mitochondria suspended in a buffer of 10mM Tris and 1mM EDTA, pH 7.4. Mitochondrial oxygen consumption was then measured at 37°C in respiration buffer (in mM: 1.5 EGTA, 3 $MgCl_2$, 10 KH_2PO_4, 20 HEPES, 110 sucrose, 20 taurine, 60 K-MES, 1 g/L BSA, pH 7.1) using a Clark-type electrode in an O2K Respirometer (Ourobouros Instruments, Austria). At the beginning of each experiment, changes in pressure, temperature, and instrumental oxygen consumption were corrected for as described by Gnaiger. Multiple respiration states were measured at 37°C as described by Siegel *et al.* using the following substrate-inhibitor combinations: proton leak (state 4; 10 mM glutamate/5 mM pyruvate/2 mM malate, without ADP), state 3 (state 4 conditions plus 2 mM ADP with and without 10 mM succinate), with fatty acid substrate (2 mM octanoyl carnitine) complex I inhibition (0.5μM rotenone), 2.5 μM antimycin A to measure non-mitochondrial oxygen consumption, and complex IV (0.5 mM N,N,N′,N′-tetramethyl-ρ-phenylenediamine (TMPD), 2 mM ascorbate, 2.5 μm antimycin A). Potassium cyanide (2 μM) is used to confirm complex IV-specific activity (94). The amount of oxygen consumed is calculated by assuming the O_2 solubility in media to be 0.920 and by calibrating initial oxygen concentration in the buffer for each experiment and correcting for pressure, temperature

and instrumental oxygen consumption as described by Gnaiger (95). Oxygen consumption was then normalized to total protein content as determined by a Bradford assay (96).

For titration experiments, precise volumes of 100mM ADP or dADP stock were injected using a Tip2K attachment (Ourorbouros Instruments) after addition of Complex I substrates and cytochrome C. Oxygen consumption was measured as soon as the rate plateaued, and titration immediately resumed. After the addition of 1500 μM ADP or dADP, the uncoupling agent Carbonyl cyanide-p-trifluoromethoxyphenylhydrazone (FCCP) was titrated until OCR plateaued to confirm maximum electron transport system activity.

4.2.7 Preparation of adenovirus

The AdEasy^{TM} system was used to generate recombinant adenoviral vectors to express Rrm1 and either Rrm2 or Rrm2B from the same cytomegalovirus promoter. A self-cleaving P2A peptide was placed between the genes for the two subunits. Green fluorescent protein (GFP) on its own CMV promoter was used as a reporter to identify transduced cells, and a GFP-only virus was used as a control. Adenovirus was amplified in HEK293T cells and titered according to the Adeno-X Rapid Titer Kit protocol (Clontech Laboratories, Mountain View, CA) using GFP to identify positive cells.

4.2.8 Adult rat cardiomyocyte isolation and adenoviral transduction

Cardiomyocytes were isolated from adult Fischer 344 rats via enzymatic digestion through retrograde aortic perfusion. The heart was rapidly excised, trimmed, and perfused with collagenase/protease solution, after which the ventricles were removed, minced, and triturated. Cells were plated on glass coverslips (for IonOptix experiments) or plastic culture dishes (for MS and WB) incubated for at least 1 hour in 0.1 mg/mL laminin in PBS. After two hours, plating media was aspirated and replaced with a minimal volume of media (~200 μL) containing adenovirus (500 ifu/cell). Additional media was added after one hour for overnight incubation. Cells were assayed three days after transduction. Measurements were performed by two different experimentalists and analyzed by the same reader.

4.2.9 Neonatal rat cardiomyocyte isolation and adenoviral transduction

Cardiomyocytes were isolated from 1-3 day old Sprague-Dawley rat pups using a protocol described previously (33). Rats were sacrificed by decapitation and the hearts rapidly excised, minced, and serially digested in buffer containing 150U/mL collagenase II (Worthington Biochemical Corporation, Lakewood, NJ) plus 0.35U/mL protease XIV (Sigma). Cells were pre-plated for 1 hour to remove fibroblasts and enrich cardiomyocyte fraction, then plated overnight in dishes coated with 1% gelatin in DMEM + 5% FBEssence (VWR). 50 ifu/cell adenovirus was then added to the media for overnight incubation. Medium was replaced the following day with DMEM with no serum and 10 μM Ara-C to inhibit growth of proliferative cells. Cells were collected for assays three days after transduction.

4.2.10 Western blot

Protein samples were solubilized in 1% NP-40 lysis buffer with 4% protease inhibitors (Sigma) and centrifuged for 14,000 g for 5 minutes. The supernatant was mixed with SDS protein sample buffer containing β-mercaptaethanol (Bio-Rad) and resolved by SDS-PAGE on 4-20% Mini-Protean GTX Stain-Free gels (Bio-Rad). Protein transfer to 0.45 mm polyvinylidene difluoride membranes was performed at constant 100 volts at 4°C in Towbin's buffer containing 20% methanol for 1 hour. Blots were blocked for 1 hour at room temperature in 1x BlockerFL (Thermo Scientific) before overnight incubation with primary antibodies (Human Rrm1: Abcam ab137114, 1:1000; Human Rrm2/Rrm2B: Sigma GW22152A, 1:1000).

4.2.11 SR calcium uptake assay

SR Ca^{2+} uptake was measured as previously described (97). Ventricles from adult mice were homogenized in ice-cold buffer (mM: 50 KH_2PO_4, 10 NaF, 1 EDTA, 300 sucrose, 0.3 PMSF, 0.5 DTT). Homogenate was added to uptake buffer (mM: 0.5 EGTA, 0.5 MgCl2, 5 MgATP, 10 creatine phosphate, 40 imidazole, 5 potassium oxalate, 5 NaN3, 10 procaine, 0.03 ruthenium red, pH 7.1) containing calcium at concentrations varying from pCa 8 to 5. After a two-minute pre-incubation of the assay buffer containing 150 μCi/mL ^{45}Ca (Perkin Elmer, Waltham, MA) at 37°C, ventricular homogenate was incubated with continuous stirring. The reaction was stopped after two minutes by filtration through a 0.45-μM Millipore filter and washed twice with cold buffer

(20 mM Tris, 2mM EGTA pH 7.0). Radioactivity was measured using a scintillation counter and normalized to protein content in the homogenate determined by Pierce BCA protein assay. Total vesicular calcium uptake was calculated by determining the amount of ^{45}Ca bound to the Millipore filters via a liquid scintillation counter. The following equation was used to determine the SR Ca^{2+} uptake rate: Ca^{2+} Uptake = nmol Ca x (counts per minute/(specific activity x 5) x 1/mg protein in 300 µL) x 0.5.

4.2.12 Statistics

The statistical analyses were performed using GraphPad Prism 8 (Graphpad Software). Comparison of echocardiography, *ex vivo* pressure development, and isolated cardiomyocytes between WT and RNRB-TG mice used student's t-test between mice of the same sex with correction for multiple comparisons. Transduced cells were compared using a paired student's t-test with correction for multiple comparisons. Results were considered statistically significant at $p \leq 0.05$. The results shown here are mean ± SEM unless otherwise stated.

4.3 RESULTS

4.3.1 Transgenic overexpression of RNRB elevates dATP in cardiac tissue

We used high-performance liquid chromatography mass spectrometry (HPLC-MS/MS) to measure total dATP and ATP content in both whole myocardium and isolated cardiomyocytes. Consistent with earlier published findings from this model, we found that the ratio of dATP to ATP were significantly elevated in myocardium in both sexes (Table 4.1).

Table 4.1 dNTP content of WT and $RNRB^{TG}$ mouse hearts.

n =4-6 mice per group. *p < 0.05 vs WT of same sex

	WT Male	$RNRB^{TG}$ Male	WT Female	$RNRB^{TG}$ Female
[dATP]/[ATP]%	0.013±0.001	0.99±0.096*	0.011±0.002	0.83±0.09*
ATP (pmol/mg)	3107±397	2475±263	3892±448	2907±473
dATP (pmol/mg)	0.40±0.05	24±3*	0.46±0.1	23±4*
dGTP(pmol/mg)	1.2±0.2	1.4±0.3	0.6±0.3	1.4±0.1*
dCTP(pmol/mg)	0.31±0.05	5.3±0.6*	0.28±0.08	4.3±1*
dTTP(pmol/mg)	0.85±0.1	0.15±0.04*	0.78±0.2	0.08±0.02*
dADP(pmol/mg)	0.19±0.04	19±10*	0.35±0.1	8.3±4*

4-month old RNRB^{TG} mice of both sexes had significantly less body weight than WT littermates, with no change in tibia length. Heart weight was significantly increased in female transgenic mice, but not in males. This resulted in a significant increase in heart weight to body weight ratio (HW/BW), but not heart weight to tibia length (HW/TL). Some of the reduction in body weight in both sexes is due to a reduction in muscle mass indicated by a reduction in the size of the gastrocnemius, the largest muscle in the hindlimb. Both sexes display a reduced ratio of gastrocnemius mass to both body weight and tibia length (Table 4.2).

Table 4.2 Descriptive statistics of animal phenotype at four months of age.

n =6-9 mice per group. *p < 0.05 vs WT of same sex.

	WT Male	RNRB^{TG} Male	WT Female	RNRB^{TG} Female
Body weight (g)	32.9±0.6	27.8±0.6*	27.0±1.2	22.4±0.5*
Heart weight (mg)	165±6	155±5	122±5	140±6*
Tibia length (mm)	19.1±0.3	18.9±0.4	18.5±0.3	18.3±0.3
Gastrocnemius (mg)	163±6	125±5*	127±6	90±4*
HW/BW	5.0±0.2	5.6±0.1*	4.5±0.2	6.3±0.2*
HW/TL	8.6±0.3	8.3±0.3	6.6±0.3	7.6±0.2*
BW/TL	1.72±0.03	1.48±0.04*	1.47±0.06	1.22±0.03*
G/TL	8.6±0.4	6.7±0.3*	7.0±0.3	5.0±0.3*
G/BW	5.0±0.2	4.5±0.1*	4.7±0.2	4.1±0.2*

4.3.2 Mice overexpressing RNRB have elevated systolic and diastolic function

Cardiac function was first assessed *in vivo* by echocardiography. Fractional shortening, and calculated ejection fraction were significantly elevated in RNRB mice (Table 4.3). No differences were found in mean E'/A' ratios in tissue doppler measurements of diastolic function. These data suggest that as previously reported, elevation of cytosolic [dATP] enhances systolic contractility without contributing to cardiac hypertrophy or impairing diastole.

Table 4.3 Echocardiogram statistics from transgenic mice. N ≥ 10 mice per group. HR: heart rate D.s: End-systolic Diameter of the left ventricle. D.d: End-diastolic Diameter of the left ventricle. EF: Ejection Fraction. FS: Fractional Shortening. LVAW;s: End-systolic Left Ventricular Anterior Wall thickness. LVPW;s: End-systolic Left Ventricular Posterior Wall thickness. *p ≤ 0.05 vs WT of the same sex.

	WT Male	$RNRB^{TG}$ Male	WT Female	$RNRB^{TG}$ Female
HR, bpm	557±12	545±7	562±10	549±10
D.s, mm	2.32±0.05	2.19±0.03*	2.19±0.05	2.04±0.05*
D.d, mm	3.83±0.05	3.79±0.03	3.58±0.05	3.55±0.05
EF, %	70±1	74±0.6*	70±1	74±0.7*
FS, %	39.3±0.9	42.0±0.6*	38.9±0.7	42.6±0.6*
LVAW;s mm	1.66±0.06	1.62±0.03	1.54±0.02	1.55±0.04
LVPW;s mm	1.18±0.04	1.27±0.02	1.18±0.06	1.13±0.03
E/A	1.5±0.3	1.9±0.1	1.6±0.2	1.7±0.1
E'/A'	1.24±0.02	1.12±0.03	1.2±0.1	1.2±0.1

We next used isolated Langendorff-perfused hearts to more precisely observe differences in kinetics of pressure development *ex vivo* in baseline and high-calcium conditions by means of a small balloon inserted into the left ventricle. Beating spontaneously, left-ventricular developed pressure was significantly increased in $RNRB^{TG}$ mice of both sexes, along with both positive and negative rates of pressure development (dP/dt), indicators of the kinetics of activation and relaxation. As there was no significant difference in heart rate between genotypes, $RNRB^{TG}$ mice had significantly higher rate-pressure product, a measure of cardiac output (Figure 4.1). High-workload challenge was induced by increasing extracellular calcium concentration from 2mM to 4mM for 20 minutes. LV developed pressure increased in both sexes of WT and male $RNRB^{TG}$ mice, as well as the maximum rates of pressure change, supporting earlier findings that RNR overexpression does not compromise the heart's ability to increase output (4, 42, 76) (Figure 4.2).

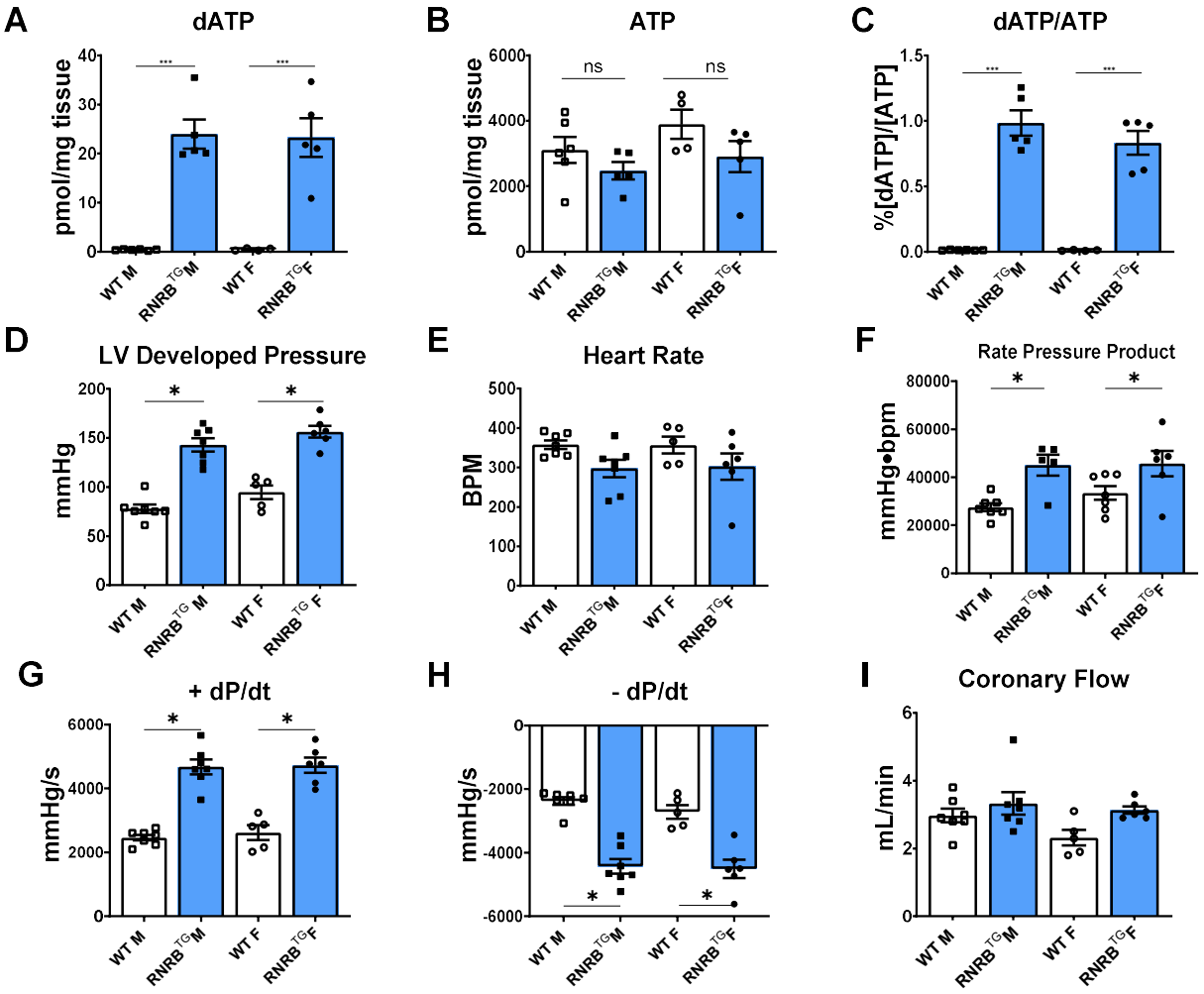

Figure 4.1 dATP content and baseline contractility in perfused isolated hearts. Both sexes of transgenic mice have significantly elevated dATP content (A) with no significant differences in ATP (B), leading to roughly 1% [dATP]/[ATP] in the myocardium (C). (D) Left-ventricular developed pressure is increased with transgenic overexpression of RNRB in both sexes with no change in spontaneous heart rate (E). Cardiac output (rate-pressure product, F) is therefore also higher. (G) The maximum rate of pressure development (+dP/dt) and relaxation (-dP/dt, H) are both increased in transgenic mice. (I) Coronary flow is estimated by collecting perfusate over a two-minute period and is unchanged in transgenic mice. N ≥ 5 mice per group. *p ≤ 0.05 vs WT of the same sex.

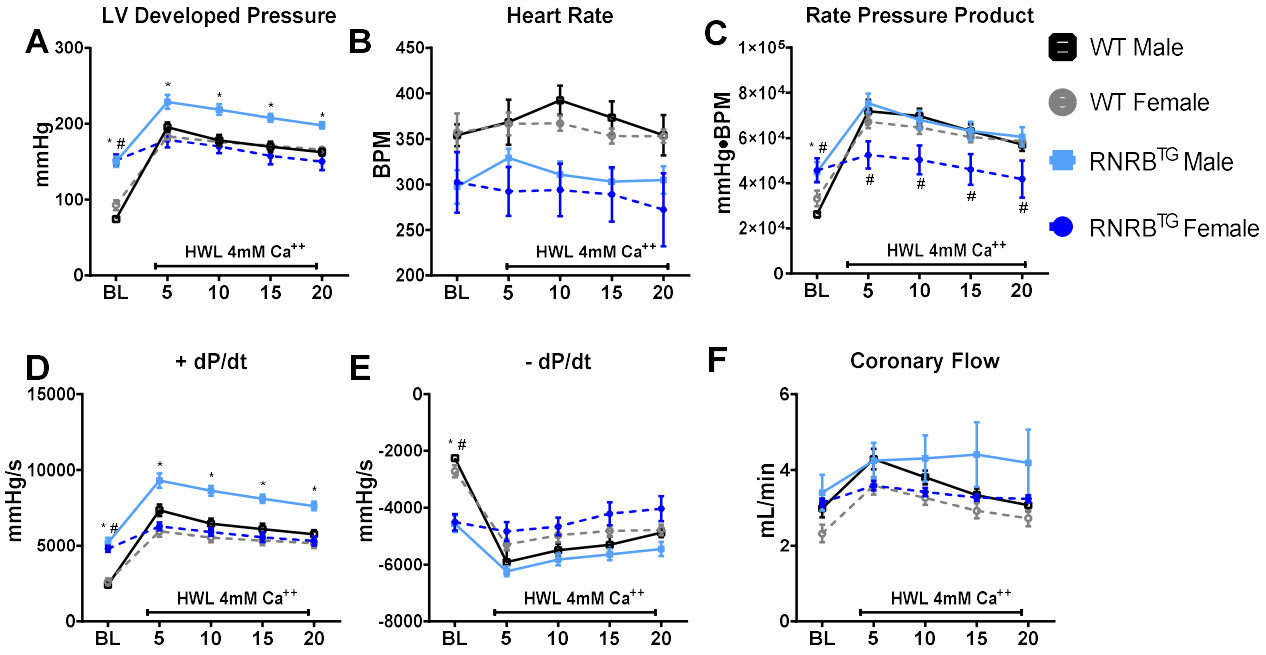

Figure 4.2 Isolated perfused hearts under high workload induced by elevating Ca^{2+}.
Left ventricular developed pressure (A) increased with elevated Ca2+ in all groups except in transgenic females. Heart rate (B) did not change with high Ca2+, but rate-pressure product (C) increased in WT males and females to equal that of RNRBTG males. (D) Transgenic males maintained higher +dP/dt compared to WT. (E) -dP/dt increased in transgenic males with high Ca2+ but was matched by the change in both sexes of WT. (F) Coronary flow did not differ between groups. N ≥ 10 mice per group. *p ≤ 0.05 vs WT of the same sex.

Unexpectedly, female $RNRB^{TG}$ mice did not respond to the high-workload challenge, and several hearts became arrhythmic when the high calcium solution was introduced (not shown). Subsequently, LV developed pressure in the transgenic female hearts was equal to wild type under high workload conditions, but significantly lower than in male transgenics. Given that baseline *ex vivo* and *in vivo* parameters are the same in both sexes, we do not currently have a working hypothesis for why females do not respond (or respond negatively) to high calcium.

4.3.3 Contractility and calcium handling are enhanced in isolated cardiomyocytes

Hearts from male $RNRB^{TG}$ mice respond less than wild-types to high-calcium challenge, especially during diastole. Hearts from female mice did not respond at all. To test whether RNRB

overexpression affects calcium handling, we isolated cardiomyocytes and measured contractility and calcium transients in single unloaded cells simultaneously using the calcium indicator fura-2. As *in vivo* and whole heart preparations, contractility was increased in isolated cells (Table 4.4). Maximum rate of contraction, fractional shortening, and maximum rate of relaxation were all significantly increased in cells isolated from transgenic mice, with no significant increase in systolic calcium. Notably, the maximum rate of calcium signal decay was greater in transgenic cells.

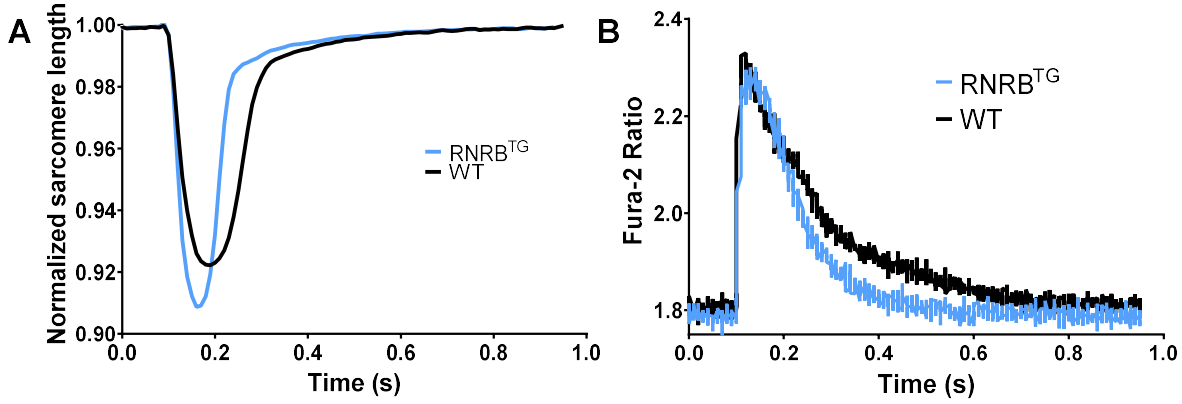

Figure 4.3 Representative traces of sarcomere length (A) and calcium transients (B) in isolated mouse cardiomyocytes.

Table 4.4 Contractile properties of isolated cardiomyocytes from transgenic mice.

N = 5-7 mice per group, n ≥57 cells per group. *p ≤ 0.05 vs WT of the same sex

	WT Male	**RNRB^{TG} Male**	**WT Female**	**RNRB^{TG} Female**
Resting sarcomere length (μm)	1.87±0.01	1.88±0.01	1.85±0.01	1.87±0.01
Fractional shortening (%)	7.3±0.2	9.0±0.3*	6.7±0.3	9.3±0.3
Maximum rate of contraction (μm/s)	-3.7±0.1	-4.5±0.1*	-2.8±0.2	-5.0±0.2*
Time to peak (ms)	83±2	73±1*	103±4	73±1*
Maximum rate of relaxation (μm/s)	2.4±0.1	3.5±0.20*	1.7±0.1	4.0±0.2*
Time to 50% relaxation (ms)	77±4	69±3	78±4	43±1*
Time to 90% relaxation (ms)	140±7	117±6	167±12	91±5*
Resting Ca^{2+} (Fura-2 ratio)	1.56±0.02	1.60±0.02	1.68±0.04	1.53±0.03*
Ca^{2+} transient amplitude (Fura-2 ratio units)	0.44±0.02	0.52±0.03	0.47±0.03	0.58±0.03
Ca^{2+} transient amplitude (% of baseline Fura-2 ratio)	28±1	32±2	28±1	37±2*
Maximum rate of Ca2+ release (U/s)	45±2	52±3	50±3	67±5
Maximum rate of Ca2+ decay (U/s)	-2.6±0.1	-3.5±0.2*	-2.6±0.2	-4.2±0.2*
Time to transient peak (ms)	33±1	35±2	35±2	31±2
Time to 50% transient decay (ms)	129±3	120±4	127±6	103±3*
Time to 90% transient decay (ms)	336±12	322±13	382±22	339±14

4.3.4 Adenoviral transduction of RNRB enhances dATP and contractility in cultured cardiomyocytes

We next performed an experiment to induce overexpression of Rrm1 and Rrm2B in cardiomyocytes to see if results from transgenic mice can be replicated in transduced cells that have not developed in elevated [dATP]. Cells were isolated from adult male Fischer 344 rats and transduced *in vitro* using an adenovirus construct containing cDNA for Rrm1 and Rrm2B linked by a P2A cleavage peptide on the same CMV promoter. Transduction was verified by inclusion of GFP on a separate CMV promoter in the viral vector. Protein expression and dATP content were verified in neonatal rat cardiomyocytes to achieve high enough cellular density for nucleotide analysis via mass spectrometry, as dNTP content in adult cardiomyocytes are in the range of femtomoles per cell. Like in the transgenic mice, rat cells overexpressing RNRB have a significantly increased [dATP]/[ATP] (Figure 4.4).

Also as in transgenic mice, transduced rat cardiomyocytes overexpressing RNRB show a significant increase in the magnitude of contraction and rates of contraction and relaxation measured by changes in sarcomere length (Figure 4.4, Table 4.5). Additionally, transduced adult rat cells showed increases in the relative magnitude and kinetics of Ca^{2+} transients using fura-2. The maximum rates of both transient signal increase (a marker of Ca^{2+} release from the SR) and decay (sequestration by SERCA and/or extrusion through the NCX) increased with overexpression of RNRB.

4.3.5 Engineering mutations in ribonucleotide reductase

Transduced overexpression of Rrm1 has been stable in our hands, but Rrm2 has been highly variable (Regnier lab unpublished data). We hypothesized that Rrm2 is degraded when overexpressed in cardiomyocytes. To test this, we engineered mutations in two sites critical to proteaseome-dependent degradation in Rrm2 (Degradation-resistant RNR, RNR-DR). Preliminary results from adenoviral transduction of adult cardiomyocytes are similar to experiments of RNRB overexpression (Table 4.5). Future experiments will compare the effects of this engineered mutation on Rrm2 overexpression, dATP production, and contractility in cultured cardiomyocytes. Our goal is to develop an improved RNR vector that will be resistant to degradation through the

ubiquitin-proteasome pathway and therefore enable more stable and consistent RNR enzyme activity and deoxynucleotide levels of cardiomyocytes transduced in vivo.

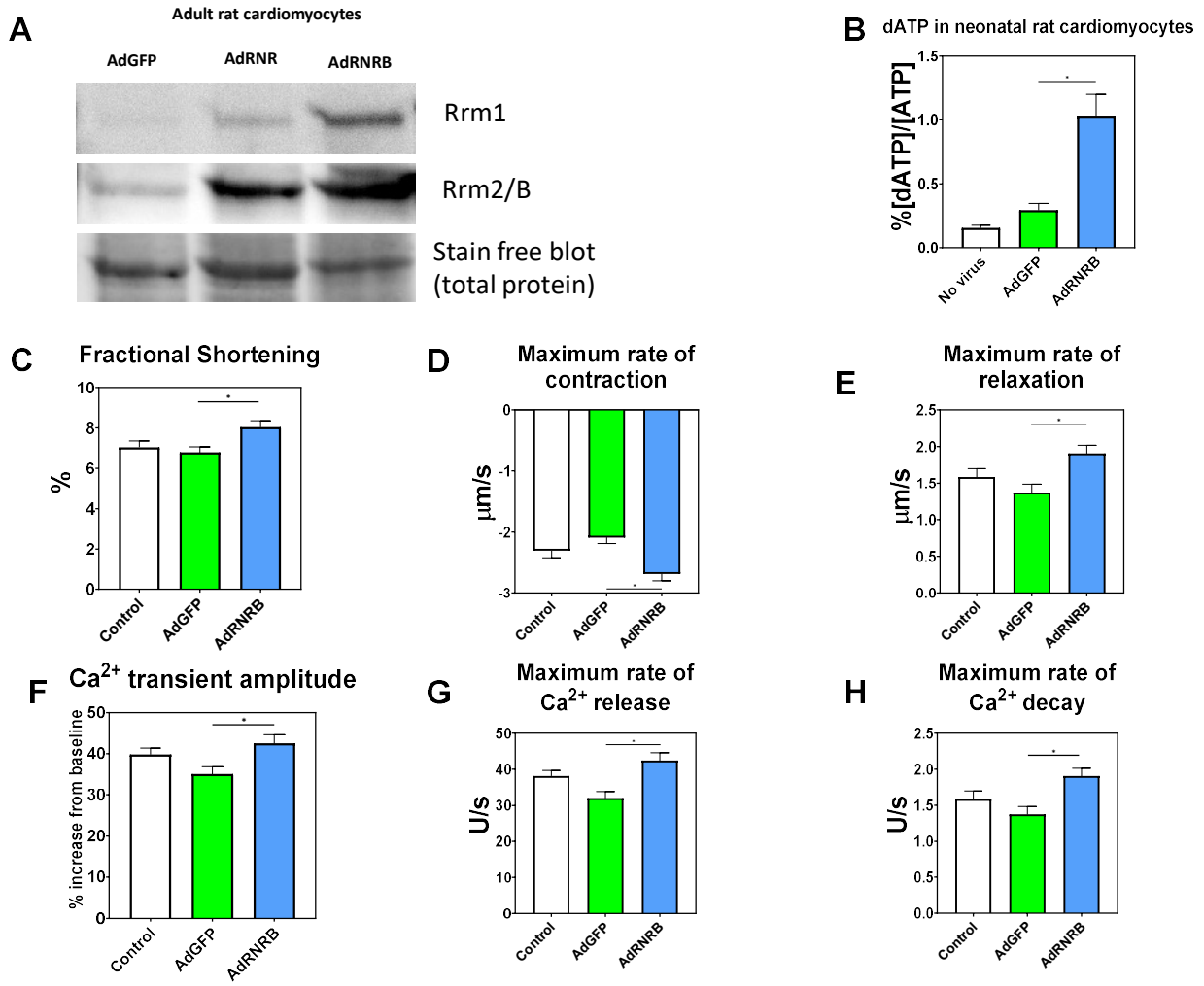

Figure 4.4 Cardiomyocytes transduced with RNRB in culture have elevated dATP and enhanced contractility and calcium handling. (A) Western blot showing expression of Rrm1 and Rrm2 or Rrm2B in transduced adult cardiomyocytes. (B) dATP is elevated in neonatal rat cardiomyocytes after adenovirus-mediated transduction of RNRB. (C-E) Contractility is enhanced in transduced adult rat cardiomyocytes stimulated at 1 Hz and 37C. (F-H) Calcium handling is also altered by overexpression of RNRB. Full details are listed in Table 4.5.

Table 4.5 Contractile properties of transduced adult rat cardiomyocytes. Adult rat cardiomyocytes transduced with all three isoforms of RNR showed increased contractility compared to controls transduced with GFP. N = 4 rats, n ≥ 20 cells per group. * $p < 0.05$ vs AdGFP.

	Control	AdGFP	AdRNRB	AdRNRDR	AdRNR
Resting sarcomere length (μm)	1.81±0.007	1.77±0.006	1.78±0.005	1.78±0.006	1.78±0.005
Fractional shortening (%)	7.0±0.3	6.8±0.3	8.0±0.3*	7.9±0.3*	8.0±0.4*
Maximum rate of contraction (μm/s)	-2.3±0.1	-2.0±0.1	-2.7±0.1*	-2.6±0.1*	-2.5±0.1*
Time to peak (ms)	137±4	135±4	120±3	126±4	130±4
Maximum rate of relaxation (μm/s)	1.6±0.1	1.4±0.1	1.9±0.1*	2.1±0.1*	1.7±0.1
Time to 50% relaxation (ms)	100±6	103±6	83±3*	78±5*	94±4
Time to 90% relaxation (ms)	190±13	204±15	166±12*	154±13*	170±10*
Resting Ca^{2+} (Fura-2 ratio)	1.0±0.01	0.94±0.01	1.06±0.01	0.98±0.02	0.99±0.01
Ca^{2+} transient amplitude (Fura-2 ratio units)					
Ca^{2+} transient amplitude (% of baseline)	40±2	38±2	44±2	49±4*	35±2
Maximum rate of Ca^{2+} release (U/s)	38±2	21±1	28±1*	43±4*	35±2
Maximum rate of Ca^{2+} decay (U/s)	-1.8±0.8	-1.6±0.08	-2.0±0.9*	-2.1±0.2*	-1.6±0.1
Time to transient peak (ms)	34±2	41±2	42±2	45±4	38±3
Time to 50% transient decay (ms)	145±3	154±3	149±3	146±4	144±5
Time to 90% transient decay (ms)	411±11	442±13	392±14*	411±21	418±19

4.3.6 dATP and SERCA

Given that the maximum rate of calcium decay is increased in both transgenic and transduced cardiomyocytes, we hypothesized that maximum Ca^{2+} uptake by SERCA may be increased with elevated dATP. This idea is supported by previously published findings by Trumble, Sutko, and Reeves that dATP can be used as a substrate in isolated sarcoplasmic reticulum vesicles (98). To

verify this hypothesis in cardiac tissue, C57/BL6 mouse hearts were homogenized and incubated with ^{45}Ca in buffers containing either ATP or dATP in buffers with pCa varying from 8 to 5 and radioactivity in the homogenate was measured using a scintillation counter (Figure 4.5). While results confirm that SERCA2 can use dATP as a substrate with similar affinity to ATP, neither total uptake (473±78 for ATP, 434±65 for dATP, arbitrary units normalized to total protein) or calcium sensitivity (pCa50, 6.59±0.03 with ATP, 6.70±0.16 with dATP) were significantly changed with nucleotide.

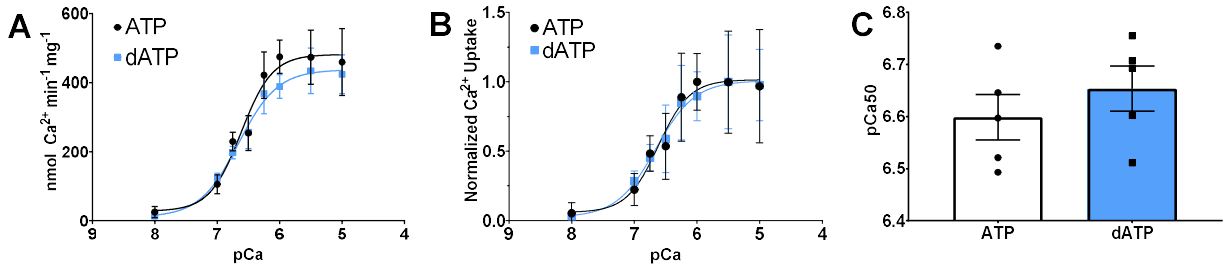

Figure 4.5 dATP does not alter Ca2+ uptake in the sarcoplasmic reticulum. (A) Uptake of ^{45}Ca in mouse heart homogenate incubated in varying [Ca^{2+}] and 5 mM ATP (black) or dATP (blue). (B) Normalized calcium uptake and(C) Ca^{2+} concentration at half-maximal activity (pCa50) are not changed with dATP. n = 5 mice.

4.3.7 Transgenic RNRB overexpression does not alter mitochondrial metabolism

Mitochondria account for over 90% of ATP production in the heart (99), so it is imperative that any therapeutic not interfere with mitochondrial ATP production. Mitochondria were enriched from the myocardium of healthy adult mice. In a sealed chamber and in the presence of metabolic substrates, the rate of oxygen consumption was measured with a Clark-type electrode while either ADP or dADP was titrated in to determine if a) dADP can be used as an effective substrate for oxidative phosphorylation and b) if the kinetics of the reaction differ from that of ADP. To eliminate the possibility of interactions between dADP and the electron transport complexes, the uncoupling agent FCCP was added to allow unregulated proton flow across the inner mitochondrial membrane and determine the maximum ADP-independent oxygen consumption.

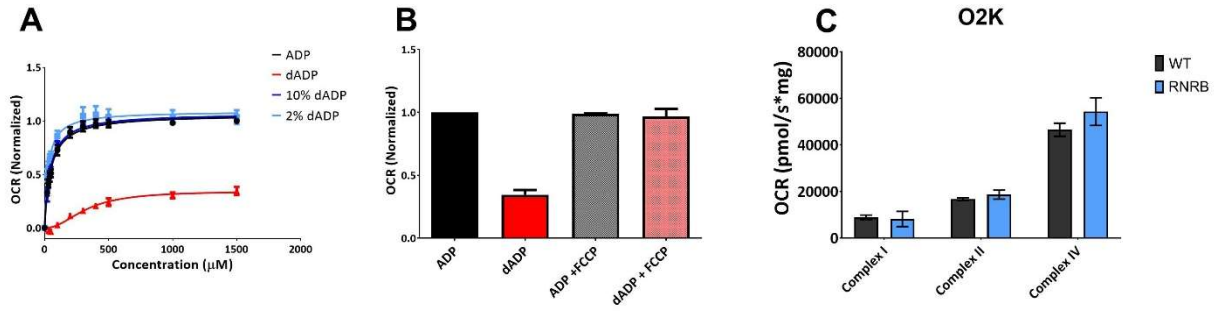

Figure 4.6 Respiratory capacity of cardiac mitochondria with elevated dADP/dATP.
(A) dATP is a less efficient substrate than ADP for oxidative phosphorylation, but physiologically relevant concentrations of dATP do not alter the kinetics or maximum rate of ADP-dependent respiration. (B) Maximum oxygen consumption rate with dADP is restored by addition of the uncoupler FCCP. (C) Mitochondrial respiratory capacity is unchanged in transgenic mice.

dADP-dependent respiration of cardiac mitochondria was depressed when compared to ADP-dependent respiration, and higher concentrations of dADP are necessary to stimulate respiration (K_{mADP} = 44±12, K_{mdADP} = 567±176). Despite this, uncoupled respiration was no different in dADP-stimulated mitochondria than in ADP-stimulated mitochondria, and dADP/ADP ratios exceeding those expected from overexpression of RNR (2% and 10% of total ADP) elicited the same magnitude of respiration as 100% ADP (Figure 4.6A-B). [ADP] in a cardiomyocyte is approximately 50 μM (100). If only 1% of total ADP in myocytes overexpressing RNR is dADP, it would not likely have a measurable effect. In addition, cardiac mitochondria from transgenic mice that overexpress RNRB have the same maximum respiratory capacity as wild-type controls (Figure 4.6C). These data suggest that levels of dADP associated with overexpression of RNR do not alter the cell's ability to synthesize ATP and that mitochondrial metabolism is unaltered by overexpression of RNRB.

4.4 Discussion

4.4.1 dATP can be elevated by multiple isoforms of RNR

Virally-mediated cardiac gene therapy has yet to fully translate the success of numerous preclinical studies into successful clinical trials for a variety of factors, especially due to ineffective delivery

of candidate genes (35, 39, 101). Ribonucleotide reductase is an appealing candidate gene for delivery because the therapeutic is not the protein but its product (dATP), which can diffuse freely through gap junctions into cells which may not have been transduced(5). In previous studies we have demonstrated effective gene transfer of RNR in both rodent and porcine models using an AAV6 construct with a cardiac troponin T-derived promotor cassette (2, 3). The purpose of this study is to investigate the therapeutic use of multiple isoforms of ribonucleotide reductase. Our lab has previously reported that both transgenic and virally mediated overexpression of RNR elevates dATP and increases cardiac performance, and that the amount of force increase scales with dATP concentration in skinned cardiac muscle. Attempting to apply this therapy to disease models has achieved mixed results, with especially problematic variability in RNR protein after transduction. We thereby hypothesize that if a more effective means of delivery is developed, we may be able to further increase intracellular [dATP] and cardiac performance.

Here we overexpressed Rrm1 together with an isoform of the small subunit (Rrm2B) which the lab had not previously utilized. Though past *in vitro* measurements found that Rrm2B has lower enzymatic activity than Rrm2 (88), dATP is sufficiently elevated in both the transgenic mouse and virally-transduced cardiomyocytes to dramatically increase cardiac contractility. Transgenic mice that overexpress Rrm1 and Rrm2B have significantly higher cardiomyocyte [dATP] as measured by liquid chromatography-mass spectrometry than wild-type littermates. This translates to increased systolic function measured by echocardiography as well as enhanced shortening and relaxation in isolated cardiomyocytes. There is also an increase in the rate of release, magnitude, and rate of decay of measured calcium transients. We believe that this dATP is phosphorylated by creatine kinase, which is very sensitive to dADP. Concentrations of dADP physiologically relevant to these mice do not stimulate oxidative phosphorylation in isolated cardiac mitochondria, and the mitochondria of these mice do not have significantly altered respiratory capacity.

Previous studies using adenoviral gene transfer used two vectors, each encoding a single subunit of the enzyme (102). In contrast, all studies of AAV-mediated transduction *in vivo* have used a single vector for both subunits linked using a P2A cleavage peptide (42, 76). Here we used the same single-vector construct design used in AAVs. Overexpression of both subunits of the enzyme increased the amount of dATP in cultured neonatal cardiomyocytes. In adult cardiomyocytes RNRB increased fractional shortening compared to controls, as well as shorter time to 50%

relaxation, offering further evidence that dATP's inotropic effect does not prolong crossbridge attachment. We were also able to recapitulate the transgenic mouse model's faster decay of Ca^{2+} transient via *in vitro* transduction of adult rat cardiomyocytes. This may be due to faster calcium release from the myofilament during relaxation, or possibly due to increased SERCA activity with dATP. Given our results showing that SERCA2a activity is not increased by dATP, we hypothesize that these changes in calcium handling are a result of faster crossbridge detachment in the sarcomere allowing Ca^{2+} to be more quickly sequestered in the SR or extruded via the NCX.

4.4.2 Mice overexpressing RNRB have more pronounced sexual dimorphism

One unexpected finding from this study is that females overexpressing RNRB systemically have markedly different performance than males. They have significantly larger reductions body weight, muscle weight, and muscle/body weight ratios compared to wild-type controls than the males. *In vivo* measurement of cardiac function by echocardiography found no difference between males and females, and baseline *ex vivo* developed pressures in isolated hearts are similar between sexes. Similarly, contractility is increased in isolated cardiomyocytes from both male and female mice overexpressing Rrm1 and Rrm2B.

Unexpectedly, female transgenic hearts failed to respond to high calcium in *ex vivo* measurement of cardiac pressure development. We hypothesize that this dimorphism is the result of differences in endocrine signaling between the sexes being exacerbated by dNTP imbalance during development. Because this transgenic line overexpresses RNRB globally, it will be difficult to determine the exact mechanism behind the change. Cardiomyocytes isolated from female rats and transduced *in vitro* with both isoforms if the small subunit overexpressed the enzyme in sufficient quantities to increase contractility. We do not anticipate cardiac-specific overexpression to interfere with endocrine function in adults. Nevertheless, we will do all future work regarding RNR overexpression in an inducible, tissue-specific manner in both sexes.

Chapter 5. OTHER CONTRIBUTIONS

5.1 FAST AND SENSITIVE HPLC-MS/MS METHOD FOR INDIRECT QUANTIFICATION OF INTRACELLULAR DEOXYRIBONUCLEOTIDE TRIPHOSPHATES FROM TISSUE AND CELLS

Olafsson, S, D Whittington, JD Murray, M Regnier, F Moussavi-Harami. 2017. Fast and sensitive HPLC-MS/MS method for direct quantification of intracellular deoxyribonucleoside triphosphates from tissue and cells. *Journal of Chromatography B*, 1068: 90-97

Deoxyribonucleotide triphosphates (dNTPs) are required for nuclear and mitochondrial DNA replication and repair. dNTP pools are tightly controlled as irregularly large concentrations of all dNTPs are associated with increased replication error and an imbalance of dNTPs is observed in a variety of disease conditions. dNTP pools are generally elevated during DNA synthesis and cell proliferation but can be extremely low in non-dividing cells such as cardiomyocytes, around 1-10 pmol per million cells and less than 1 pmol in the mitochondria. Previously used methods for nucleotide and deoxynucleotide quantification have relatively low sensitivity and require an impractical sample volume to yield accurate results in cardiomyocytes, so we developed a new robust, sensitive, and specific assay using HPLC-MS/MS for quantifying dNTPs along with ATP in tissues and isolated cells.

Our assay is capable of quantifying endogenous dNTP content in various tissues with considerably lower variability than enzymatic assays. By using chromatographic buffers that exclude ion-pairing reagents and using ammonium hydroxide in the organic solvent, our lower level of quantification using this method is 62.5 femtomoles for all four dNTPs, at least 4-fold more sensitive than the lowest previously published value of 0.25 picomoles. We have successfully used this method to quantify dATP in whole myocardium, freshly isolated cardiomyocytes, and cultured cardiomyocytes.

5.2 TIME-RESOLVED X-RAY DIFFRACTION AND MOLECULAR DYNAMICS STUDIES OF SKELETAL MUSCLE RELAXATION WITH 2-DEOXY-ATP

Small molecules that target striated muscle myosin are being actively pursued as possible treatments for conditions that result in hypo- or hypercontractility (22, 24). Myosin activators can work by increasing recruitment of myosin S1-heads toward the thin filaments and/or by altering the dynamics of the actin-myosin crossbridge cycle, such as prolongation of actin-myosin attachment time. However, augmentation of contraction by activators may come at the cost of altered or impaired relaxation (17, 23, 25, 103–105), a critical aspect of muscle function dependent on the rate of actin-myosin crossbridge detachment. An ideal trait for myosin activators would be to enhance contraction without retarding relaxation. Patients with preserved ejection fraction but abnormal diastolic relaxation account for about half of hospitalizations due to heart failure (7). An ideal therapeutic inotrope would be effective in treating both systolic and diastolic dysfunction. Because dATP interacts directly with the myosin, understanding the molecular mechanisms by which it affects contraction and relaxation may not only determine its potential as a therapeutic agent, it may also be instructive of beneficial structure-function changes for other potential myosin targeted molecular compounds being considered to treat hypo-contractile muscle. To the best of our knowledge, dATP is the only myosin activator which increases the magnitude of force production without prolonging relaxation. A more complete understanding of the relationship between the changes in the structure and function of dATP-bound myosin may inform its potential as a therapeutic and assist in the search for other potential therapeutic compounds which target the thick filament.

Muscle relaxation is traditionally assessed by kinetics derived from force decay profiles, but the drop to baseline force is not necessarily concurrent with full relaxation of myosin heads and readiness for a new binding cycle. In this study we have combined time-resolved x-ray diffraction, the only technique that allow studying molecular level (nanometer) events under physiological conditions at high time resolution (millisecond-scale), with molecular dynamics (MD) simulations of the post-power stroke state of myosin to study how dATP affects relaxation after myosin heads have detached from actin in transgenic mice that overexpress RNR (106). We chose to use soleus muscle for these experiments because 1) the more ordered structure of skeletal muscle (compared to cardiac muscle) allows higher resolution imaging of structural features, and 2) it shares

approximately 40% of its myosin (MYH7; β-myosin)(107, 108) and troponin C (TNNC1; cTnC) isoforms with cardiac tissues via slow twitch muscle fibers(109). X-ray studies were performed in the beamline (18ID) at the Advanced Photon Source at Argonne National Laboratory for real-time monitoring of sarcomere structures and the intensity of myosin layer lines during tetanic contraction and relaxation in intact muscle simultaneously with force measurements.

Previous simulations suggest that dADP is less stable than ADP in the binding pocket and may be released faster. As P_i release is the rate-limiting step in the cross-bridge cycle, this could explain how dATP increases rates of both relaxation and contraction in cardiac muscle. For this study, all molecular dynamics simulations were done by Matthew Childers. X-ray diffraction of intact mouse soleus muscle was designed, executed, and analyzed by Weikang Ma. I performed measurements of nucleotide content in mouse soleus and determination of skeletal muscle myosin isoforms.

To our knowledge, this is the first study to examine relaxation rates in mammalian skeletal muscle using x-ray diffraction with high time resolution under physiological conditions.

As in cardiac muscle, $I_{1,1}/I_{1,0}$ was elevated in resting soleus, indicating that the myosin heads are in a state primed for contraction even with ~1% [dATP]/[ATP]. As this state is still helically ordered, it is possible that the faster return of MLL1 intensity is due to the heads moving a shorter distance. dADP-bound myosin also maintains an increased affinity for actin after the powerstroke, which may explain slowed relaxation.

Our findings suggest that with even 1% dATP, myosin heads adopt a pre-power stroke configuration that favors crossbridge attachment, likely due to an increase in increase in positively-charged residues in the actin binding site (83). We also observed that myosin heads return to an ordered relaxed state more quickly as evidenced by x-ray diffraction data. MD simulations of post-power stroke myosin containing either ADP or dADP demonstrate changes in contact pairs between the nucleotide and amino acids in the binding pocket, which are associated with greater mobility and dADP that may increase its rate of release. These local structural changes appear to precipitate changes out to the actin binding surface of myosin that reduces its affinity for actin to accelerate crossbridge detachment.

Chapter 6. CONCLUSIONS AND FUTURE DIRECTIONS

The research presented in this dissertation builds on over a decade of previous work to develop deoxy-ATP as a therapeutic for cardiomyopathy. The goals were to determine the molecular mechanisms by which dATP increases force production and increased rates of contraction and relaxation in striated muscle and to improve the targeted delivery of ribonucleotide reductase by overexpression of alternate isoforms of the enzyme's small subunits.

6.1 dATP INCREASES FORCE PRODUCTION IN CARDIAC MUSCLE BY ALTERING ELECTROSTATIC INTERACTIONS BETWEEN ACTIN AND MYOSIN

Molecular dynamics simulations of the S1 myosin head suggested that the presence of dADP*P_i in the nucleotide binding pocket causes the actin-binding surface of myosin adopts an alternate configuration with a greater number of exposed positive charges. We hypothesized that this would increase the affinity of myosin for actin binding and used a combination of Brownian dynamics simulations and x-ray diffraction to test our hypothesis.

BrownDye simulations showed that probability of actin-myosin interaction was higher with dADP*Pi in the binding pocket than ADP*P_i at all reaction distances tested. This can be attributed to a higher number of positively charged residues on the binding surface and a correspondingly higher number of contact pairs between residues that were able to form.

X-ray diffraction of demembranated cardiac trabeculae showed that incubation of the muscle in dATP caused the myosin heads to adopt a configuration similar to a partially activated state even at rest. The 1,1/1,0 intensity ratio indicates the relative distribution of mass between the thick and thin filaments and is significantly increased with the addition of dATP. This effect was diminished when we increased electrostatic interactions between the filaments by lowering the ionic strength of the surrounding solution. The difference was also abolished by activating the muscles with sub-maximal calcium, which is consistent with the hypothesis that dATP primes the thick filament by perturbing the myosin heads and increasing weak binding of myosin at resting calcium.

6.2 COMBINATORIAL GENE THERAPY PRESERVES SKELETAL MUSCLE FUNCTION IN MDX MICE

In a pilot study of combinatorial gene therapy for Duchenne muscular dystrophy, AAV-mediated transduction of dystrophin-deficient mice preserved skeletal muscle function into young adulthood, an effect that is likely due primarily to microdystrophin expression. Both groups that received microdystrophin had preserved hindlimb strength compared to untreated controls, but mdx mice transduced with RNR alone unexpectedly displayed an exacerbated disease phenotype. dATP was only elevated in mice which received both vectors, which suggests that RNR-transduced cells had not survived in the group that did not receive microdystrophin. While this study focused primarily on skeletal muscle outcomes, cardiomyocytes were isolated from a subset of animals. Fractional shortening was lower in microdystrophin-transduced cardiomyocytes compared to untreated controls, which was restored when combined with RNR treatment with no change in calcium transient amplitude. These findings suggest that microdystrophin may increase stiffness in transduced cardiomyocytes, but that a combinatorial gene therapy may be more effective for preserving cardiac function than dystrophin replacement alone.

6.3 OVEREXPRESSION OF RRM1 AND RRM2B ELEVATES DATP AND CARDIAC PERFORMANCE IN TRANSGENIC MICE AND CULTURED CELLS

dNTP synthesis is regulated by cell cycle-dependent degradation of the small subunit, Rrm2. Several studies of AAV-mediated delivery of RNR *in vivo* have yielded consistent overexpression of Rrm1 but extremely variable levels of Rrm2 in transduced myocardium when measured by Western blot. We hypothesized that this is due to degradation of the small subunit after translation. There is another isoform of the small subunit, called Rrm2B or p53R2, which is present in nondividing cells and has been shown to be necessary for DNA repair and mitochondrial homeostasis. Here, we used a transgenic mouse model with global overexpression of both Rrm1 and Rrm2B as well as cultured adult rat cardiomyocytes *in vivo* to explore whether Rrm2B overexpression will also elevate cytosolic [dATP] and subsequently enhance cardiac function.

Transgenic overexpression of Rrm1 and Rrm2B indeed elevated cardiac [dATP] and contractility both *in vivo* and *in vitro.* The mice showed a mild increase in ejection fraction measured by

echocardiography, but a pronounced increase in left-ventricular developed pressure measured in spontaneously beating hearts *ex vivo*. Maximum rates of positive and negative pressure change were also significantly elevated *ex vivo.*

Contractility was also increased in isolated cardiomyocytes, both from transgenic mice and isolated adult rat cardiomyocytes transduced with Rrm1 and Rrm2B in culture. The changes in contractile kinetics were accompanied by an unexpected increase in the maximum rate of calcium transient decay. There is some evidence that SERCA2 can use dATP as a substrate for ATPase activity, but experiments comparing the two nucleotides showed no difference in either maximum rate of calcium reuptake or changes in calcium sensitivity with dATP.

6.4 FUTURE DIRECTIONS

6.4.1 Exploration of RNR as therapeutic in skeletal muscle

One of the hallmarks of heart failure is exercise intolerance. Cardiac dysfunction can be mediated through exercise, but the increase in cardiac output in response to exercise begins to decline in middle age and continues throughout life (110). This decrease in cardiac reserve contributes significantly to exercise intolerance in the elderly, which further exacerbates the issue and leads to a reduction in quality of life. Multiple human trials have shown that an increase in cardiac output in heart failure patients, if chronically maintained, leads to a subsequent increase in exercise tolerance (111–113).

Skeletal muscle myosin can also use dATP as a substrate for force production, but with different outcomes than cardiac muscle. Calcium sensitivity is slightly increased in skeletal muscle with dATP, but force at maximum calcium is unchanged. When *in vivo* measurements of hindlimb force production and fatigue resistance with direct muscle stimulation were made in our RNRB-TG mice, we found no difference in the force-frequency relationship of stimulation to force or in maximum force produced. Likewise, soleus muscles of transgenic mice with elevated dATP developed the same force at the same rates when stimulated *ex vivo.* It seems likely that dATP's augmentation of force production is dependent on the unique cooperativity between myosin crossbridges in cardiac muscle and that skeletal muscle myopathies are not promising targets for therapeutic elevation of RNR.

6.4.2 Tissue-specific inducible transgenic mice will maximize targeted RNR elevation in adult animals

Virally mediated transduction efficiency may never reach 100%. AAV-mediated overexpression is a promising avenue for therapeutic use, but transgenic animals remain desirable research models. Though we have focused on their cardiac function, all transgenic mice used in our studies of RNR to date have overexpressed the genes globally; the extra copies of Rrm1 and Rrm2/Rrm2B have been inserted into the genome with a cytomegalovirus promoter, meaning that RNR and subsequently dATP have been elevated in every cell in the body. This presumably can lead to differences in development, as relative and absolute concentrations of dNTPs can have a significant effect on cellular processes. Are RNRB-TG mice thinner because they have higher cardiac output, and are more active? Are differences in fiber types related to cardiac function, or hormonal signaling during development? Does RNR overexpression alter brain development or behavior? It would be difficult, if not impossible, to isolate the contributions of a single process or organ system to these changes.

Tissue-specific inducible transgenic lines can be used to overexpress RNR in a single cell type and answer some of these questions in both cardiac and skeletal muscle. The Regnier lab is working to create a transgenic mouse line with RNR overexpression linked to the alpha-myosin heavy chain promoter, the primary isoform of cardiac myosin found in mice. This will enable better characterization of dATP's maximum effect in the adult heart without altering development.

6.5 ALTERNATIVE METHODS OF RNR DELIVERY

6.5.1 Protein engineering

Ribonucleotide reductase activity, especially with the Rrm2 small subunit, is closely linked to DNA synthesis, and multiple pathways regulate protein levels in both dividing and quiescent cells. We have presented evidence that altering the small subunit overexpressed can increase dATP levels using either naturally occurring isoforms or engineered mutations that introduce resistance to degradation.

A known mutation exists in the large subunit (Rrm1 D57N) which alters the allosteric inhibition of enzyme activity by elevated dATP concentration. In transgenic lines this mutation elevates dATP tenfold above simple overexpression but is embryonic lethal when overexpressed in mice. Attempts to engineer a transgenic mouse expressing the D57N isoform result in births far below Mendelian ratios, but viral overexpression is a potential avenue for elevating dATP beyond 1% of the total ATP pool in cardiomyocytes.

6.5.2 Promotor engineering

Delivery is still the biggest hurdle to successful gene therapies. The work presented here focuses on transgenic mice and cells transduced *in vitro* (and even use of Rrm2B) because of the difficulty and expense of delivering high concentrations of virus to hearts *in vivo.* Previous studies of RNR gene therapy have exclusively used a promotor derived from cardiac troponin T. Recent studies summarized here and continuing in the Regnier lab have used viruses with a CK8 promotor which is expressed in both cardiac and skeletal muscles, and direct comparisons have shown that tissues transduced with CK8 have higher levels of dATP after four weeks (Regnier lab unpublished data). Later iterations of the CK8 promotor that are still in early stages of use promise to be even more effective. Given that we have found no ill effects of elevated dATP in skeletal muscle, future studies will utilize the greater transduction efficiency of these promotors coupled with more carefully selected isoforms of RNR.

6.5.3 hiPSC-CM implantation

Human induced pluripotent stem cells (hiPSC) are another potential delivery mechanism for dATP. Patient-derived cell therapy obviates the need for immune suppression after transplants. Many problems remain to be solved, including but not limited to differentiating hiPSCs into cardiomyocytes at larger scales and shorter time frames, improving survival of implanted cells, and integration with the recipient myocardium. Once integrated, hiPSC-derived cardiomyocytes overexpressing RNR could deliver dATP to the rest of the heart, improving both systolic and diastolic function.

BIBLIOGRAPHY

1. Moussavi-Harami F, et al. (2015) 2-Deoxy adenosine triphosphate improves contraction in human end-stage heart failure. *J Mol Cell Cardiol* 79:256–63.

2. Kolwicz SC, et al. (2015) AAV6-mediated Cardiac Specific Over-expression of Ribonucleotide Reductase Enhances Myocardial Contractility. *Mol Ther*. doi:10.1038/mt.2015.176.

3. Kadota S, et al. (2015) Ribonucleotide reductase-mediated increase in dATP improves cardiac performance via myosin activation in a large animal model of heart failure. *Eur J Heart Fail* 17(8):772–781.

4. Nowakowski SG, et al. (2013) Transgenic overexpression of ribonucleotide reductase improves cardiac performance. *Proc Natl Acad Sci U S A* 110(15):6187–92.

5. Lundy SD, et al. (2014) Cell-based delivery of dATP via gap junctions enhances cardiac contractility. *J Mol Cell Cardiol* 72:350–9.

6. Nowakowski SG, Regnier M, Daggett V (2017) Molecular mechanisms underlying deoxy-ADP.Pi activation of pre-powerstroke myosin. *Protein Sci* 26(4):749–762.

7. Benjamin EJ, et al. (2019) Heart Disease and Stroke Statistics—2019 Update: A Report From the American Heart Association. *Circulation* 139(10). doi:10.1161/cir.0000000000000659.

8. Strait JB, Lakatta EG (2012) Aging-associated cardiovascular changes and their relationship to heart failure. *Heart Fail Clin* 8(1):143–64.

9. Quarles EK, et al. (2015) Quality control systems in cardiac aging. *Ageing Res Rev*. doi:10.1016/j.arr.2015.02.003.

10. Biernacka A, Frangogiannis NG (2011) Aging and Cardiac Fibrosis. *Aging Dis* 2(2):158–173.

11. Hamdani N, Paulus WJ (2013) Myocardial titin and collagen in cardiac diastolic dysfunction: partners in crime. *Circulation* 128(1):5–8.

12. Feridooni H a., Dibb KM, Howlett SE (2014) How cardiomyocyte excitation, calcium release and contraction become altered with age. *J Mol Cell Cardiol*:1–11.

13. Fernandez-Sanz C, et al. (2014) Defective sarcoplasmic reticulum-mitochondria calcium exchange in aged mouse myocardium. *Cell Death Dis* 5:e1573.

14. Loffredo FS, Nikolova AP, Pancoast JR, Lee RT (2014) Heart failure with preserved ejection fraction: molecular pathways of the aging myocardium. *Circ Res* 115(1):97–107.

15. Maughan DW (2005) Kinetics and Energetics of The Crossbridge Cycle. *Heart Fail Rev* 10(3):175–185.

16. Moss RL, Razumova M, Fitzsimons DP (2004) Myosin Crossbridge Activation of Cardiac Thin Filaments. *Circ Res* 94(10):1290–1300.

17. Bakkehaug JP, et al. (2015) The Myosin Activator Omecamtiv Mecarbil Increases Myocardial Oxygen Consumption and Impairs Cardiac Efficiency Mediated by Resting Myosin ATPase Activity. *Circ Heart Fail*:CIRCHEARTFAILURE.114.002152-.

18. Liu Y, White HD, Belknap B, Winkelmann DA, Forgacs E (2015) Omecamtiv Mecarbil Modulates the Kinetic and Motile Properties of Porcine β-Cardiac Myosin. *Biochemistry* 54(10). doi:10.1021/bi5015166.

19. Nagy L, et al. (2015) The novel cardiac myosin activator omecamtiv mecarbil increases the calcium sensitivity of force production in isolated cardiomyocytes and skeletal muscle fibres of the rat. *Br J Pharmacol* 172(18):4506–4518.

20. Hashem S, Tiberti M, Fornili A (2017) Allosteric modulation of cardiac myosin dynamics by omecamtiv mecarbil. *PLOS Comput Biol* 13(11):e1005826.

21. Greenberg BH, et al. (2015) Safety and Tolerability of Omecamtiv Mecarbil During Exercise in Patients With Ischemic Cardiomyopathy and Angina. *JACC Hear Fail* 3(1):22–29.

22. Mamidi R, et al. (2017) Dose-Dependent Effects of the Myosin Activator Omecamtiv Mecarbil on Cross-Bridge Behavior and Force Generation in Failing Human Myocardium. *Circ Heart Fail*. doi:10.1161/CIRCHEARTFAILURE.117.004257.

23. Planelles-Herrero VJ, Hartman JJ, Robert-Paganin J, Malik FI, Houdusse A (2017) Mechanistic and structural basis for activation of cardiac myosin force production by omecamtiv mecarbil. *Nat Commun* 8(1):190.

24. Cleland JG, et al. (2011) The effects of the cardiac myosin activator, omecamtiv mecarbil, on cardiac function in systolic heart failure: a double-blind, placebo-controlled, crossover, dose-ranging phase 2 trial. *Lancet* 378(9792):676–683.

25. Swenson AM, et al. (2017) Omecamtiv Mecarbil Enhances the Duty Ratio of Human β-Cardiac Myosin Resulting in Increased Calcium Sensitivity and Slowed Force Development in Cardiac Muscle. *J Biol Chem* 292(9):3768–3778.

26. Reconditi M (2006) Recent improvements in small angle x-ray diffraction for the study of muscle physiology. *Reports Prog Phys* 69(10):2709–2759.

27. Martyn D, et al. (2004) Response of Equatorial X-Ray Reflections and Stiffness to Altered Sarcomere Length and Myofilament Lattice Spacing in Relaxed Skinned Cardiac Muscle. *Biophys J* 86(February):1002–1011.

28. Reconditi M (2006) Recent improvements in small angle x-ray diffraction for the study of muscle physiology. *Reports Prog Phys* 69(10):2709–2759.

29. Kinoshita Y, Nishigaki K (1997) Unexpectedly general replaceability of ATP in ATP-requiring enzymes. *J Biochem* 122(1):205–11.

30. Regnier M, Homsher E (1998) The effect of ATP analogs on posthydrolytic and force development steps in skinned skeletal muscle fibers. *Biophys J* 74(6):3059–71.

31. Regnier M, Martyn DA, Chase PB (1998) Calcium regulation of tension redevelopment kinetics with 2-deoxy-ATP or low [ATP] in rabbit skeletal muscle. *Biophys J* 74(4):2005–15.

32. Regnier M, Lee DM, Homsher E (1998) ATP analogs and muscle contraction: mechanics and kinetics of nucleoside triphosphate binding and hydrolysis. *Biophys J* 74(6):3044–58.

33. Korte FS, et al. (2011) Upregulation of cardiomyocyte ribonucleotide reductase increases intracellular 2 deoxy-ATP, contractility, and relaxation. *J Mol Cell Cardiol* 51(6):894–901.

34. Brignole EJ, et al. (2018) 3.3-Å resolution cryo-EM structure of human ribonucleotide reductase with substrate and allosteric regulators bound. *Elife* 7:1–23.

35. Dunbar CE, et al. (2018) Gene therapy comes of age. *Science* 359(6372):eaan4672.

36. Ylä-Herttuala S (2012) Endgame: Glybera Finally Recommended for Approval as the First Gene Therapy Drug in the European Union. *Mol Ther* 20(10):1831–1832.

37. Greenberg B, et al. (2016) Calcium upregulation by percutaneous administration of gene therapy in patients with cardiac disease (CUPID 2): a randomised, multinational, double-blind, placebo-controlled, phase 2b trial. *Lancet* 387(10024):1178–1186.

38. Penny WF, Hammond HK (2017) Randomized Clinical Trials of Gene Transfer for Heart Failure with Reduced Ejection Fraction. *Hum Gene Ther* 28(5):378–384.

39. Greenberg B, et al. (2014) Design of a Phase 2b Trial of Intracoronary Administration of AAV1/SERCA2a in Patients With Advanced Heart Failure: The CUPID 2 Trial (Calcium Up-Regulation by Percutaneous Administration of Gene Therapy in Cardiac Disease Phase 2b). *JACC Hear Fail* 2(1):84–92.

40. Ishikawa K, Weber T, Hajjar RJ (2018) Human Cardiac Gene Therapy. *Circ Res* 123(5):601–613.

41. Hulot J-S, et al. (2017) Effect of intracoronary administration of AAV1/SERCA2a on ventricular remodelling in patients with advanced systolic heart failure: results from the AGENT-HF randomized phase 2 trial. *Eur J Heart Fail* 19(11):1534–1541.

42. Kolwicz SC, et al. (2019) Gene Therapy Rescues Cardiac Dysfunction in Duchenne Muscular Dystrophy Mice by Elevating Cardiomyocyte Deoxy-Adenosine Triphosphate. *JACC Basic to Transl Sci* d. doi:10.1016/j.jacbts.2019.06.006.

43. Regnier M, Rivera AJ, Chen Y, Chase PB (2000) 2-deoxy-ATP enhances contractility of rat cardiac muscle. *Circ Res* 86(12):1211–7.

44. Regnier M, et al. (2004) Cross-bridge versus thin filament contributions to the level and rate of force development in cardiac muscle. *Biophys J* 87(3):1815–24.

45. Huber GA, McCammon JA (2010) Browndye: A Software Package for Brownian Dynamics. *Comput Phys Commun* 118(11):1896–1905.

46. Fischetti R, et al. (2004) The BioCat undulator beamline 18ID: A facility for biological non-crystalline diffraction and X-ray absorption spectroscopy at the Advanced Photon Source. *J Synchrotron Radiat* 11(5):399–405.

47. Jiratrakanvong J, Ma W, Agam G, Irving T (2018) *MuscleX : a new tool for analyzing X-ray diffraction patterns from muscle and other fibrous systems* doi:10.1107/S0108767318098707.

48. Dolinsky TJ, Nielsen JE, McCammon JA, Baker NA (2004) PDB2PQR: An automated pipeline for the setup of Poisson-Boltzmann electrostatics calculations. *Nucleic Acids Res* 32(WEB SERVER ISS.):665–667.

49. Baker NA, Sept D, Joseph S, Holst MJ, McCammon JA (2001) Electrostatics of nanosystems: Application to microtubules and the ribosome. *Proc Natl Acad Sci* 98(18):10037–10041.

50. Luty BA, McCammon JA, Zhou H (1992) Diffusive reaction rates from Brownian dynamics simulations: Replacing the outer cutoff surface by an analytical treatment. *J Chem Phys* 97(8):5682–5686.

51. Razumova M V., et al. (2006) Effects of the N-terminal domains of myosin binding protein-C in an in vitro motility assay: Evidence for long-lived cross-bridges. *J Biol Chem* 281(47):35846–35854.

52. Kron SJ, Toyoshima YY, Uyeda TQP, Spudich JABT-M in E (1991) Assays for actin sliding movement over myosin-coated surfaces. *Molecular Motors and the Cytoskeleton* (Academic Press), pp 399–416.

53. Pardee JD, Spudich JA (1982) Purification of muscle actin. *Methods Enzymol* 85 Pt B:164–81.

54. Spudich JA, et al. (1982) Actin and Myosin: Control of Filament Assembly [and Discussion]. *Philos Trans R Soc B Biol Sci* 299(1095):247–261.

55. Gordon AM, LaMadrid MA, Chen Y, Luo Z, Chase PB (1997) Calcium regulation of skeletal muscle thin filament motility in vitro. *Biophys J* 72(3):1295–1307.

56. Homsher E, Wang F, Sellers JR (1992) Factors affecting movement of F-actin filaments propelled by skeletal muscle heavy meromyosin. *Am J Physiol* 262(3):C714–C723.

57. Furch M, Geeves MA, Manstein DJ (1998) Modulation of actin affinity and actomyosin adenosine triphosphatase by charge changes in the myosin motor domain. *Biochemistry* 37(18):6317–6326.

58. Xu S, Martyn D, Zaman J, Yu LC (2006) X-ray diffraction studies of the thick filament in permeabilized myocardium from rabbit. *Biophys J* 91(10):3768–3775.

59. Furch M, Geeves MA, Manstein DJ (1998) Modulation of Actin Affinity and Actomyosin Adenosine Triphosphatase by Charge Changes in the Myosin Motor Domain †. *Biochemistry* 37(18):6317–6326.

60. Alamo L, et al. (2008) Three-Dimensional Reconstruction of Tarantula Myosin Filaments Suggests How Phosphorylation May Regulate Myosin Activity. *J Mol Biol* 384(4):780–797.

61. Woodhead JL, et al. (2005) Atomic model of a myosin filament in the relaxed state. *Nature* 436(7054):1195–1199.

62. Colson B a, et al. (2008) Protein kinase A-mediated phosphorylation of cMyBP-C increases proximity of myosin heads to actin in resting myocardium. *Circ Res* 103(3):244–51.

63. Colson BA, et al. (2012) Myosin binding protein-C phosphorylation is the principal mediator of protein kinase A effects on thick filament structure in myocardium. *J Mol Cell Cardiol* 53(5):609–616.

64. Kampourakis T, Yan Z, Gautel M, Sun Y-B, Irving M (2014) Myosin binding protein-C activates thin filaments and inhibits thick filaments in heart muscle cells. *Proc Natl Acad Sci* 111(52):18763–18768.

65. Zoghbi ME, Woodhead JL, Moss RL, Craig R (2008) Three-dimensional structure of vertebrate cardiac muscle myosin filaments. *Proc Natl Acad Sci* 105(7):2386–2390.

66. Colson BA, et al. (2010) Differential roles of regulatory light chain and myosin binding protein-C phosphorylations in the modulation of cardiac force development. *J Physiol* 588(6):981–993.

67. Reconditi M, et al. (2017) Myosin filament activation in the heart is tuned to the mechanical task. *Proc Natl Acad Sci*:201619484.

68. Caremani M, et al. (2019) Inotropic interventions do not change the resting state of myosin motors during cardiac diastole. *J Gen Physiol* 151(1):53–65.

69. Tanner BCW, Daniel TL, Regnier M (2012) Filament Compliance Influences Cooperative Activation of Thin Filaments and the Dynamics of Force Production in Skeletal Muscle. *PLoS Comput Biol* 8(5):e1002506.

70. Smith L, Tainter C, Regnier M, Martyn DA (2009) Cooperative Cross-Bridge Activation of Thin Filaments Contributes to the Frank-Starling Mechanism in Cardiac Muscle. *Biophys J* 96(9):3692.

71. Gordon AM, Homsher E, Regnier M (2000) Regulation of contraction in striated muscle. *Physiol Rev* 80(2):853–924.

72. Greenberg BH, et al. (2015) Safety and tolerability of omecamtiv mecarbil during exercise in patients with ischemic cardiomyopathy and angina. *JACC Hear Fail* 3(1):22–29.

73. Malik FI, et al. (2011) Cardiac myosin activation: A potential therapeutic approach for systolic heart failure. *Science (80-)* 331(March):1439–1443.

74. Winkelmann DA, Forgacs E, Miller MT, Stock AM (2015) Structural basis for drug-induced allosteric changes to human β-cardiac myosin motor activity. *Nat Commun* 6. doi:10.1038/ncomms8974.

75. Kampourakis T, Zhang X, Sun Y-B, Irving M (2017) Omecamtiv Mercabil and Blebbistatin modulate cardiac contractility by perturbing the regulatory state of the myosin filament. *J Physiol* 00:1–16.

76. Kolwicz SC, et al. (2016) AAV6-mediated cardiac-specific overexpression of ribonucleotide reductase enhances myocardial contractility. *Mol Ther* 24(2):240–250.

77. Romitti PA, et al. (2015) Prevalence of Duchenne and Becker Muscular Dystrophies in the United States. *Pediatrics* 135(3):513–521.

78. Bachrach E, et al. (2004) Systemic delivery of human microdystrophin to regenerating mouse dystrophic muscle by muscle progenitor cells. *Proc Natl Acad Sci U S A* 101(10):3581–6.

79. Gregorevic P, et al. (2006) rAAV6-microdystrophin preserves muscle function and extends lifespan in severely dystrophic mice. *Nat Med* 12(7):787–789.

80. Shin J-H, et al. (2013) Microdystrophin Ameliorates Muscular Dystrophy in the Canine Model of Duchenne Muscular Dystrophy. *Mol Ther* 21(4):750–757.

81. Ylikallio E, et al. (2010) Ribonucleotide reductase is not limiting for mitochondrial DNA copy number in mice. *Nucleic Acids Res* 38(22):8208–18.

82. Whitehead NP, et al. (2016) Validation of ultrasonography for non-invasive assessment of diaphragm function in muscular dystrophy. *J Physiol* 594:7215–7227.

83. Powers JD, et al. (2019) Cardiac myosin activation with 2-deoxy-ATP via increased electrostatic interactions with actin. *Proc Natl Acad Sci*:201905028.

84. Lai Y, et al. (2009) Dystrophins carrying spectrin-like repeats 16 and 17 anchor nNOS to the sarcolemma and enhance exercise performance in a mouse model of muscular dystrophy. *J Clin Invest* 119(3):624–635.

85. Hakim CH, et al. (2017) A Five-Repeat Micro-Dystrophin Gene Ameliorated Dystrophic Phenotype in the Severe DBA/2J-mdx Model of Duchenne Muscular Dystrophy. *Mol Ther - Methods Clin Dev* 6:216–230.

86. Seto JT, Ramos JN, Muir L, Chamberlain JS, Odom GL (2012) Gene replacement therapies for duchenne muscular dystrophy using adeno-associated viral vectors. *Curr Gene Ther* 12(3):139–51.

87. Vigen R, Maddox TM, Allen LA (2012) Aging of the United States population: impact on heart failure. *Curr Heart Fail Rep* 9(4):369–74.

88. Qiu W, Zhou B, Darwish D, Shao J, Yen Y (2006) Characterization of enzymatic properties of human ribonucleotide reductase holoenzyme reconstituted in vitro from hRRM1, hRRM2, and p53R2 subunits. *Biochem Biophys Res Commun* 340(2):428–434.

89. Yen Y, Chu B, Yen C, Shih J, Zhou B (2006) Enzymatic property analysis of p53R2 subunit of human ribonucleotide reductase. *Adv Enzyme Regul* 46(1):235–247.

90. Cho E-C, et al. (2015) RRM2B-Mediated Regulation of Mitochondrial Activity and Inflammation under Oxidative Stress. *Mediators Inflamm* 2015:287345.

91. Zhou B, et al. (2003) The human ribonucleotide reductase subunit hRRM2 complements p53R2 in response to UV-induced DNA repair in cells with mutant p53. *Cancer Res* 63(20):6583–94.

92. Liu X, Xue L, Yen Y (2008) Redox Property of Ribonucleotide ReductaseSmall Subunit M2 and p53R2 (Humana Press), pp 195–206.

93. Olafsson S, Whittington D, Murray J, Regnier M, Moussavi-Harami F (2017) Fast and sensitive HPLC–MS/MS method for direct quantification of intracellular deoxyribonucleoside triphosphates from tissue and cells. *J Chromatogr B* 1068–1069:90–97.

94. Siegel MP, et al. (2011) Reduced coupling of oxidative phosphorylation in vivo precedes electron transport chain defects due to mild oxidative stress in mice. *PLoS One* 6(11):e26963.

95. Gnaiger E (2009) Capacity of oxidative phosphorylation in human skeletal muscle: new perspectives of mitochondrial physiology. *Int J Biochem Cell Biol* 41(10):1837–45.

96. Bradford MM (1976) A rapid and sensitive method for the quantitation of microgram quantities of protein utilizing the principle of protein-dye binding. *Anal Biochem* 72:248–54.

97. Lehman SJ, et al. (2019) Chronic Calmodulin-Kinase II Activation Drives Disease Progression in Mutation-Specific Hypertrophic Cardiomyopathy. *Circulation* 139(12):1517–1529.

98. Trumble WR, Sutko JL, Reeves JP (1981) Cardiac Sarcolemmal and Substrate Specificities. *J Biol Chem* 256(14):7101–7104.

99. Harris DA, Das AM (1991) Control of mitochondrial ATP synthesis in the heart. *Biochem J* 280(3):561–573.

100. Caras IW, Martin DW (1988) Molecular cloning of the cDNA for a mutant mouse ribonucleotide reductase M1 that produces a dominant mutator phenotype in mammalian cells. *Mol Cell Biol* 8(7):2698–2704.

101. Ylä-Herttuala S, Baker AH (2017) Cardiovascular Gene Therapy: Past, Present, and Future. *Mol Ther* 25(5):1095–1106.

102. Korte FS, Feest ER, Razumova M V, Tu A-Y, Regnier M (2012) Enhanced Ca2+ binding of cardiac troponin reduces sarcomere length dependence of contractile activation independently of strong crossbridges. *Am J Physiol Heart Circ Physiol* 303(7):H863-70.

103. Planelles-Herrero VJ, Hartman JJ, Robert-Paganin J, Malik FI, Houdusse A (2017) Mechanistic and structural basis for activation of cardiac myosin force production by omecamtiv mecarbil. *Nat Commun* 8(1):190.

104. Higashiyama A, Watkins MW, Chen Z, LeWinter MM (1995) Effects of EMD 57033 on contraction and relaxation in isolated rabbit hearts. *Circulation* 92(10):3094–3104.

105. Morgan BP, et al. (2010) Discovery of omecamtiv mecarbil the first, selective, small molecule activator of cardiac myosin. *ACS Med Chem Lett* 1(9):472–477.

106. Ylikallio E, et al. (2010) Ribonucleotide reductase is not limiting for mitochondrial DNA copy number in mice. *Nucleic Acids Res* 38(22):8208–8218.

107. Augusto V, Padovani CR, Rocha Campos GE (2004) *Skeletal muscle fiber types in C57Bl6J mice* Available at: http://citeseerx.ist.psu.edu/viewdoc/download?doi=10.1.1.470.4709&rep=rep1&type=pdf [Accessed April 4, 2019].

108. Wigston DJ, English AW (1992) Fiber-type proportions in mammalian soleus muscle during postnatal development. *J Neurobiol* 23(1):61–70.

109. Wang YP, Fuchs F (1994) Length, force, and Ca(2+)-troponin C affinity in cardiac and slow skeletal muscle. *Am J Physiol Physiol* 266(4):C1077–C1082.

110. Shioi T, Inuzuka Y (2012) Aging as a substrate of heart failure. *J Cardiol* 60(6):423–8.

111. Leier C V., Huss P, Magorien RD, Unverferth D V. (1983) Improved exercise capacity and differing arterial and venous tolerance during chronic isosorbide dinitrate therapy for congestive heart failure. *Circulation* 67(4):817–822.

112. Vescovo G, et al. (1998) Improved Exercise Tolerance After Losartan and Enalapril in Heart Failure : Correlation With Changes in Skeletal Muscle Myosin Heavy Chain Composition. *Circulation* 98(17):1742–1749.

113. Marzo KP, Herrmann HC, Mancini DM (1993) Effect of balloon mitral valvuloplasty on exercise capacity, ventilation and skeletal muscle oxygenation. *J Am Coll Cardiol* 21(4):856–65.